The Astrophysical Journal, 605:105–126, 2004 April 10

THE STELLAR POPULATIONS OF LOW-LUMINOSITY ACTIVE GALACTIC NUCLEI. I. GROUND-BASED OBSERVATIONS[1]

Roberto Cid Fernandes,[2] Rosa M. González Delgado,[3] Henrique Schmitt,[4,5,6] Thaisa Storchi-Bergmann,[7] Lucimara P. Martins,[8,9] Enrique Pérez,[3] Timothy Heckman,[10,11] Claus Leitherer,[8] and Daniel Schaerer[12,13]

Received 2003 July 2; accepted 2003 December 23

ABSTRACT

We present a spectroscopic study of the stellar populations of low-luminosity active galactic nuclei (LLAGNs). Our main goal is to determine whether the stars that live in the innermost (100 pc scale) regions of these galaxies are in some way related to the emission-line properties, which would imply a link between the stellar population and the ionization mechanism. High signal-to-noise ratio, ground-based long-slit spectra in the 3500–5500 Å interval were collected for 60 galaxies: 51 LINERs and LINER/H II transition objects, two starburst galaxies, and seven nonactive galaxies. In this paper, the first of a series, we (1) describe the sample; (2) present the nuclear spectra; (3) characterize the stellar populations of LLAGNs by means of an empirical comparison with normal galaxies; (4) measure a set of spectral indices, including several absorption-line equivalent widths and colors indicative of stellar populations; and (5) correlate the stellar indices with emission-line ratios that may distinguish between possible excitation sources for the gas. Our main findings are as follows: (1) Few LLAGNs have a detectable young ($\lesssim 10^7$ yr) starburst component, indicating that very massive stars do not contribute significantly to the optical continuum. In particular, no features due to Wolf-Rayet stars were convincingly detected. (2) High-order Balmer absorption lines of H I (HOBLs), on the other hand, are detected in ~40% of LLAGNs. These features, which are strongest in 10^8–10^9 yr intermediate-age stellar populations, are accompanied by diluted metal absorption lines and bluer colors than other objects in the sample. (3) These intermediate-age populations are very common (~50%) in LLAGNs with relatively weak [O I] emission ($[\mathrm{O\ I}]/\mathrm{H}\alpha \leq 0.25$) but rare (~10%) in LLAGNs with stronger [O I]. This is intriguing since LLAGNs with weak [O I] have been previously hypothesized to be "transition objects" in which both an AGN and young stars contribute to the emission-line excitation. Massive stars, if present, are completely outshone by intermediate-age and old stars in the optical. This happens in at least a couple of objects where independent UV spectroscopy detects young starbursts not seen in the optical. (4) Objects with predominantly old stars span the whole range of [O I]/Hα values, but (5) sources with significant young and/or intermediate-age populations are nearly all (~90%) weak–[O I] emitters. These new findings suggest a link between the stellar populations and the gas ionization mechanism. The strong–[O I] objects are most likely true LLAGNs, with stellar processes being insignificant. However, the weak–[O I] objects may comprise two populations, one where the ionization is dominated by stellar processes and another where it is governed by either an AGN or a more even mixture of stellar and AGN processes. Possible stellar sources for the ionization include weak starbursts, supernova remnants, and evolved poststarburst populations. These scenarios are examined and constrained by means of complementary observations and detailed modeling of the stellar populations in forthcoming communications.

Subject headings: galaxies: active — galaxies: nuclei — galaxies: starburst — galaxies: stellar content

On-line material: color figures

1. INTRODUCTION

Low-ionization nuclear emission line regions, better known as LINERs, were first described as a separate class of galaxies by Heckman (1980). These objects have characteristically strong low-ionization forbidden lines of [O I], [N II], [S II], and [O II] that distinguish them from both Seyfert and starburst nuclei. Because of their small luminosities compared to Seyfert galaxies and quasars, these objects are often called low-luminosity active galactic nuclei (LLAGNs). LLAGNs are the most common form of nuclear activity in the local universe. In the magnitude-limited survey by Ho, Filippenko, & Sargent (1995, 1997, hereafter HFS97), they comprise $\sim\frac{1}{3}$ of all galaxies.

[1] Based on observations made with the Nordic Optical Telescope, operated on the island of La Palma jointly by Denmark, Finland, Iceland, Norway, and Sweden, in the Spanish Observatorio del Roque de los Muchachos of the Instituto de Astrofísica de Canárias.

[2] Departamento de Física-CFM, Universidade Federal de Santa Catarina, C.P. 476, 88040-900, Florianópolis, SC, Brazil; cid@astro.ufsc.br.

[3] Instituto de Astrofísica de Andalucía (CSIC), P.O. Box 3004, 18080 Granada, Spain; rosa@iaa.es, eperez@iaa.es.

[4] National Radio Astronomy Observatory, 520 Edgemont Road, Charlottesville, VA 22903; hschmitt@nrao.edu.

[5] Jansky Fellow.

[6] Visiting Astronomer, Kitt Peak National Observatory, National Optical Astronomy Observatory, which is operated by AURA, Inc., under a cooperative agreement with the National Science Foundation.

[7] Instituto de Física, Universidade Federal do Rio Grande do Sul, C.P. 15001, 91501-970, Porto Alegre, RS, Brazil; thaisa@if.ufrgs.br.

[8] Space Telescope Science Institute, 3700 San Martin Drive, Baltimore, MD 21218; martins@stsci.edu, leitherer@stsci.edu.

[9] Instituto de Astronomía, Geofísica e Ciencias Atmosféricas, 05508-900 Sao Paulo, Brazil.

[10] Department of Physics and Astronomy, Johns Hopkins University, Baltimore, MD 21218; heckman@pha.jhu.edu.

[11] Also Adjunct Astronomer at STScI.

[12] Observatoire de Genève, Chemin des Maillettes 51, CH-1290 Sauverny, Switzerland.

[13] Laboratoire d'Astrophysique, UMR 5572, 14 Avenue Edouard Belin, F-31400 Toulouse, France.

What powers LLAGNs, and how do they fit in the global picture of AGNs? Are they all truly "dwarf Seyfert galaxies" powered by accretion onto nearly dormant supermassive black holes ("dead QSOs"), or can some of them be explained at least partly in terms of stellar process?

These questions have been at the forefront of AGN research for over two decades. Nowadays there is no doubt that a substantial fraction of these nuclei contain bona fide AGNs. Among the most solid evidence in support of this "AGN model" is the fact that $\sim\frac{1}{5}$ of LLAGNs have broad (few thousand kilometers per second) Hα emission (HFS97), signaling the presence of a broad-line region, a hallmark of AGNs. In fact, some of the most compelling evidence for the existence of nuclear accretion disks comes from LLAGNs with double-peaked broad Balmer lines (e.g., NGC 1097, Storchi-Bergmann et al. 1995; M81, Bower et al. 1996). X-ray observations (Terashima et al. 2000; Ho et al. 2001) and the detection of compact nuclear radio emission (Falcke et al. 2000; Nagar et al. 2000) also support the AGN model. Similarities between LLAGNs and Seyfert galaxies were also identified in the properties of their host galaxies (Ho, Filippenko, & Sargent 2003). In the theoretical front, it has long been known that photoionization by a typical AGN can reproduce the characteristic LINER emission-line spectrum (Ferland & Netzer 1983; Halpern & Steiner 1983). These and other evidence (see Barth 2002 and references therein) have contributed to the general understanding that many, maybe most, LLAGNs are bona fide members of the AGN family, the low-luminosity cousins of Seyfert galaxies.

Despite this general consensus, for nearly as long as LINERs have existed in the literature, it has been suspected that they constitute a rather mixed bag of phenomena (e.g., Filippenko 1996; Heckman 1996). LINER-like spectra are known to occur in as diverse environments as cluster cooling flows (e.g., Heckman et al. 1989; Donahue & Voit 1991), starburst-driven superwinds (Heckman, Armus, & Miley 1990), and the bulges of early-type galaxies (e.g., Heckman 1996) besides the nuclei of galaxies. It is therefore likely that a variety of ionization mechanisms are capable of producing a LINER-type spectrum, and indeed several models not involving photoionization by an AGN have been proposed to explain the emission-line characteristics of these objects. Among them are shocks (Heckman 1980; Dopita & Sutherland 1995), which may be associated with supernova remnants (SNRs), photoionization by unusually hot young stars (Filippenko & Terlevich 1992; Shields 1992; Barth & Shields 2000), or photoionization by post-AGB stars (Binette et al. 1994; Taniguchi, Shioya, & Murayama 2000). Even in nuclei where an AGN is conclusively known to exist, it is unclear what its role is in the gas ionization and in the overall energetics, since the AGN may coexist with one or more of these other ionizing agents. For instance, C IV and Si IV P Cygni lines from O stars were detected in the space-UV for a few LLAGNs by Maoz et al. (1998), lending support to the idea that at least some of these objects may be powered by young stars. Yet, in some of these same nuclei, like NGC 4569 and NGC 4594, an AGN has been detected by *Chandra* observations (Ho et al. 2001). These nuclei therefore contain both a compact starburst and an AGN. NGC 4303, recently studied by Colina et al. (2002) and Jiménez-Bailon et al. (2003), is another example. This coexistence of a starburst and an AGN is reminiscent of the starburst plus Seyfert 2 composites discussed by Heckman et al. (1997), González Delgado et al. (1998), Storchi-Bergmann, Cid Fernandes, & Schmitt (1998), González Delgado, Heckman, & Leitherer (2001), Cid Fernandes et al. (2001a), and Joguet et al. (2001).

The question then arises of what are the relative roles of accretion and other processes in the energetics of LLAGNs and how to segregate nuclei where accretion is the dominant energy source from those whose emission lines are powered mainly by stars or their remnants. HFS97 addressed this issue by dividing LLAGNs into two subclasses: "pure" or "normal" LINERs and LINER/H II "transition objects" (TOs), whose emission-line ratios are intermediate between those of LINERs and H II regions. The fundamental distinction between LINERs and TOs is the relative strength of the [O I] λ6300 line (e.g., [O I]/Hα). This collisionally excited line arises in warm neutral gas and as such is weak in gas that is photoionized by the soft radiation from O stars, since the transition between the external cold neutral gas and internal ionized layers is very sharp. In contrast, an AGN produces highly energetic photons that penetrate deeply into (and heat) the neutral gas. Although useful, the division of LLAGNs into LINERs and TOs is largely arbitrary, given that there is no clear-cut gap between LINERs and H II nuclei in the [O I]/Hα ratio.

The idea when the TO class was introduced was, in the words of HFS97, that "TOs can be most naturally explained as normal LINERs whose integrated spectra are diluted or contaminated by neighboring H II regions" (see also Ho, Filippenko, & Sargent 1993; Gonçalves, Véron, & Véron-Cetty 1999). Accordingly, the most popular models for these sources involve photoionization by hot stars in a weak nuclear starburst (Shields 1992; Filippenko & Terlevich 1992; Barth & Shields 2000), although mechanical heating by supernovae (SNe) following a short-duration burst (Engelbracht et al. 1998; Alonso Herrero et al. 2000) and photoionization by evolved "poststarburst" populations (Taniguchi et al. 2000) have also been invoked to explain their emission-line properties.

Given that so many different mechanisms are capable of producing a similar emission-line spectrum, it is evident that emission-line data per se will not be able to distinguish between different models.

In this paper and others in this series we examine the stellar populations in a sample of LLAGNs in search of clues of their nature. A simple motivation for this is that all alternative non-AGN models discussed above share a common trait: they all involve stars in one way or another, be they young and massive (a starburst), older and not so massive (poststarburst models), or massive but dead (SNR shocks). Characterizing the stellar populations of LLAGNs may thus provide us with the extra information needed to assess the relevance of the proposed scenarios.

With this central goal in mind, we have carried out a spectroscopic survey of LINERs and TOs in the 3500–5500 Å interval. This spectral range contains several stellar population features of interest, including the Wolf-Rayet (W-R) bump at 4680 Å (an unambiguous signpost of the presence of young [$<10^7$ yr] massive stars), high-order Balmer absorption lines (HOBLs) of H I (which signal the presence of evolved starbursts, from 10^7 up to 10^9 yr), the 4000 Å break, the Balmer jump, and several metal lines typical of old populations, such as Ca II K, the G band, and others. A detailed scrutiny of these features by means of stellar population analysis provides a *direct* test of models proposed for LINERs and TOs. This technique can be contrasted with the mostly used *indirect* approach of comparing emission-line ratios with predictions from photoionization or shock models.

TABLE 1

SAMPLE PROPERTIES

Galaxy Name (1)	Spectral Class (2)	Hubble Type (3)	T Type (4)	v (km s^{-1}) (5)	Distance (Mpc) (6)	pc arcsec^{-1} (pc) (7)	$\log L_{H\alpha}$ (ergs s^{-1}) (8)	[O I]/Hα (9)
NGC 266.....	L1.9	SB(rs)ab	2.0	4662	62.4	302	39.30	0.280c
NGC 315.....	L1.9	E+:	−4.0	4935	65.8	319	39.55	0.590
NGC 404.....	L2	SA(s)0−:	−3.0	−46	2.4	11	37.63	0.170
NGC 410.....	T2:	E+:	−4.0	5295	70.6	342	39.43	0.097u
NGC 428.....	L2/T2:	SAB(s)m	9.0	1160	14.9	72	36.98L	0.190u
NGC 521.....	T2/H:	SB(r)bc	4.0	5039	67.0	324	39.16	0.086c
NGC 660.....	T2/H:	SB(s)a pec	1.0	852	11.8	57	38.89	0.047
NGC 718.....	L2	SAB(s)a	1.0	1734	21.4	103	38.45	0.210
NGC 772[a]	H/T2:	SA(s)b	3.0	2458	32.6	158	39.24	0.026b
NGC 841.....	L1.9:	(R′)SAB(s)ab	2.1	4539	59.5	288	39.11L	0.580b
NGC 1052.....	L1.9	E4	−5.0	1499	17.8	86	39.45r	0.710
NGC 1161.....	T1.9:	SA0	−2.0	1940	25.9	125	38.70	0.140u
NGC 1169.....	L2	SAB(r)b	3.0	2386	33.7	163	38.67	0.320
NGC 2681.....	L1.9	(R′)SAB(rs)0/a	0.0	688	13.3	64	38.83L	0.190b
NGC 2685[a]	S2/T2:	(R)SB0+pec	−1.0	820	16.2	78	38.66	0.130b
NGC 2911.....	L2	SA(s)0: pec	−2.0	3183	42.2	204	39.38r	0.310
NGC 3166.....	L2	SAB(rs)0/a	0.0	1344	22.0	106	39.10	0.270
NGC 3169.....	L2	SA(s)a pec	1.0	1234	19.7	95	39.02	0.280
NGC 3226.....	L1.9	E2: pec	−5.0	1321	23.4	113	38.93	0.590
NGC 3245.....	T2:	SA(r)0?	−2.0	1348	22.2	107	39.59	0.086c
NGC 3627.....	T2/S2	SAB(s)b	3.0	727	6.6	31	38.50	0.130
NGC 3705.....	T2	SAB(r)ab	2.0	1018	17.0	82	38.66	0.079b
NGC 4150.....	T2	SA(r)0?	−2.0	43	9.7	47	38.18	0.130
NGC 4192.....	T2	SAB(s)ab	2.0	−142	16.8	81	38.97	0.140
NGC 4438.....	L1.9	SA(s)0/a:	0.0	64	16.8	81	39.37	0.270
NGC 4569.....	T2	SAB(rs)ab	2.0	−235	16.8	81	40.28r	0.062
NGC 4736.....	L2	(R)SA(r)ab	2.0	307	4.3	20	37.81r	0.240
NGC 4826.....	T2	(R)SA(rs)ab	2.0	411	4.1	19	38.87r	0.073
NGC 5005.....	L1.9	SAB(rs)bc	4.0	948	21.3	103	39.47	0.650
NGC 5055.....	T2	SA(rs)bc	4.0	504	7.2	34	38.62r	0.170u
NGC 5377.....	L2	(R)SB(s)a	1.0	1792	31.0	150	39.18	0.250
NGC 5678.....	T2	SAB(rs)b	3.0	1924	35.6	172	39.19	0.079
NGC 5879.....	T2/L2	SA(rs)bc?	4.0	772	16.8	81	38.32	0.160
NGC 5921.....	T2	SB(r)bc	4.0	1479	25.2	122	39.15r	0.110
NGC 5970.....	L2/T2:	SB(r)c	5.0	1965	31.6	153	38.06	0.180c
NGC 5982.....	L2::	E3	−5.0	2904	38.7	187	38.46c	0.490u
NGC 5985.....	L2	SAB(r)b	3.0	2518	39.2	190	38.94	0.300
NGC 6340.....	L2	SA(s)0/a	0.0	1207	22.0	106	38.50	0.430b
NGC 6384.....	T2	SAB(r)bc	4.0	1667	26.6	128	38.12	0.150u
NGC 6482.....	T2/S2::	E:	−5.0	3921	52.3	253	39.23	0.130u
NGC 6500.....	L2	SAab:	1.7	2999	39.7	192	40.31	0.230
NGC 6501.....	L2::	SA0+:	−0.5	2869	39.6	191	38.01c	0.870u
NGC 6503.....	T2/S2:	SA(s)cd	6.0	42	6.1	29	37.56	0.080
NGC 6702.....	L2::	E:	−5.0	4712	62.8	304	38.61c	0.620u
NGC 6703.....	L2::	SA0−	−2.5	2364	35.9	174	38.51	0.360u
NGC 6951[b]	S2	SAB(rs)bc	4.0	1424	24.1	116	39.07	0.230
NGC 7177.....	T2	SAB(r)b	3.0	1147	18.2	88	38.94	0.140
NGC 7217.....	L2	(R)SA(r)ab	2.0	945	16.0	77	38.86	0.250
NGC 7331.....	T2	SA(s)b	3.0	821	14.3	69	38.49	0.097u
NGC 7626.....	L2::	E: pec	−5.0	3422	45.6	221	38.81	0.220u
NGC 7742.....	T2/L2	SA(r)b	3.0	1653	22.2	107	39.07	0.130
NGC 3367.....	H	SB(rs)c	5.0	3041	43.6	211	40.98	0.031
NGC 6217.....	H	(R)SB(rs)bc	4.0	1362	23.9	115	40.41	0.032
NGC 205.....	Normal	dE5 pec	−5.0	−239	0.7	3	<34.79r	...
NGC 221.....	Normal	E2	−6.0	−205	0.7	3	<36.16r	...
NGC 224.....	Normal	SA(s)b	3.0	−298	0.7	3	...	...
NGC 628.....	Normal	SA(s)c	5.0	655	9.7	3	<36.69r	...
NGC 1023.....	Normal	SB(rs)0−	−3.0	632	10.5	51	<37.82r	...
NGC 2950.....	Normal	(R)SB(r)0	−2.0	1337	23.3	204	<38.42r	...
NGC 6654.....	Normal	(R′)SB(s)0/a	0.0	1823	29.5	123	<38.11r	...

NOTES.—Col. (1): Galaxy name. Col. (2): Spectral class. Col. (3): Hubble type. Col. (4): Numerical Hubble type. Col. (5): Radial velocity. Col. (6): Distance. Col. (7): Angular scale. Col. (8): Hα luminosity. Col. (9): [O I]/Hα flux ratio. All quantities were extracted from HFS97. Revised values of $\log L_{H\alpha}$, taken from Ho et al. 2003, are indicated by an "r" in col. (8). See HFS97 for the meaning of other notes on cols. (8) and (9).

[a] Grouped among TOs in this paper.

[b] Grouped with LINERs in this paper (see Pérez et al. 2000).

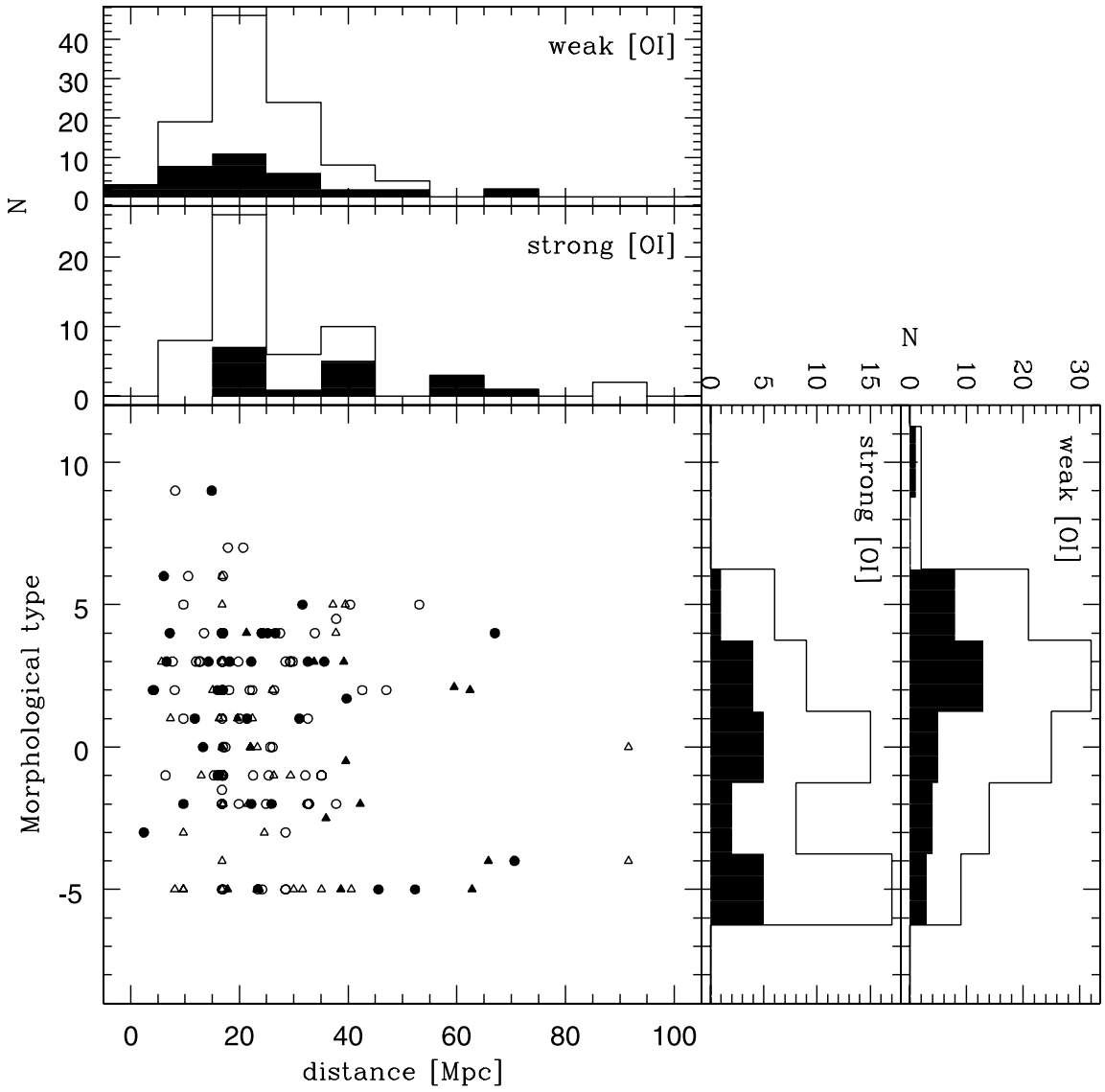

FIG. 1.—Distances and morphological T types for the strong–[O I] (*triangles*; [O I]/H$\alpha > 0.25$) and weak–[O I] LLAGNs (*circles*; [O I]/H$\alpha \leq 0.25$) in the HFS97 sample. Filled symbols and filled areas in the histograms indicate objects in our sample. (All data are extracted from HFS97.) [*See the electronic edition of the Journal for a color version of this figure*.]

Our survey is based on the sample of HFS97 but differs from it in two important aspects: wavelength coverage and spatial resolution. Unlike HFS97, we do not reach the red part of the spectrum, which includes emission lines that are the basis of spectral classification. On the other hand, the HFS97 spectra start at 4230 Å, whereas our data go down to 3500 Å. This near-UV edge contains several key stellar population diagnostics (like the HOBLs) that have not been systematically studied in previous LLAGN surveys. As shown here, results obtained in this spectral range give us a new perspective on the nature of these galaxies.

In this paper we concentrate on the presentation of the data. Companion papers will discuss stellar population synthesis analysis (González Delgado et al. 2004, hereafter Paper II), spatial gradients of spectral properties, morphology, emission-line properties, and models. This paper is organized as follows: In §§ 2 and 3 we describe the sample, observations, and reduction process. In § 4 the nuclear spectra are presented. A suite of properties has been measured from these spectra, such as equivalent widths and colors. These are presented in § 5, which also compares our measurements with previously published results. This section also presents an objective definition of the pseudocontinuum used to measure stellar population indices in Bica's system. In § 6 we examine the most important finding of this investigation: the strong connection between stellar population and emission-line properties in LLAGNs. Finally, § 7 summarizes our results.

2. SAMPLE

We selected galaxies from the Ho et al. (1995) and HFS97 sample for this study because it is the most complete and homogeneous survey of LLAGNs available and provides a representative population of galaxies in the local universe. HFS97 divided LLAGNs into two subclasses: "pure" or "normal" LINERs and LINER/H II TOs, whose emission-line ratios are intermediate between those of LINERs and H II regions. Some Seyfert galaxies also match the usual definition of LLAGNs, $L_{\rm H\alpha} < 10^{40}$ ergs s^{-1}, but in this paper "LLAGNs" is used as a synonym for LINERs and TOs. HFS97 distinguish LINERs from TOs by the value of the [O I]

$\lambda6300/H\alpha$ emission line ratio: they define LINERs as nuclei with $[O\ I]/H\alpha \geq 0.17$, while for TOs $0.08 \leq [O\ I]/H\alpha < 0.17$. Because of its sensitivity to the high-energy part of the ionizing spectrum, the $[O\ I]/H\alpha$ ratio is a good indicator of the presence of an AGN.

LINERs and TOs are further distinguished from Seyfert and H II nuclei on the basis of other line ratios: $[O\ III]\ \lambda5007/H\beta < 3$, $[N\ II]\ \lambda6583/H\alpha \geq 0.6$, and $[S\ II]\ \lambda\lambda6716, 6731/H\alpha \geq 0.4$. According to these criteria, the HFS97 survey contains 94 LINERs and 65 TOs. We have added three other galaxies to these lists: NGC 772 (classified as "H/T2:" by HFS97, i.e., a hybrid between an H II nucleus and a TO) and NGC 2685 ("S2/T2:") were grouped among TOs, while NGC 6951 (classified as a Seyfert 2 by HFS97 and as a Seyfert 2/LINER by Pérez et al. 2000) was grouped among LINERs. With these additions the HFS97 survey contains 162 LLAGNs. This sample is hereafter called the "HFS97 sample."

We have observed a subset of 28 LINERs and 23 TOs, which corresponds to $\sim\frac{1}{3}$ of the HFS97 sample. For comparison purposes, we also observed seven normal galaxies and two starburst nuclei, which gives a total of 60 galaxies. Table 1 lists the galaxies in our sample, along with several properties extracted from HFS97. As in HFS97, LINERs are listed as either L2 (if they contain only narrow lines) or L1.9 (if a broad $H\alpha$ was detected), and similarly for TOs. The L2/T2 and T2/L2 mixed classes are used when a galaxy looks more like a LINER than like a TO and vice versa, respectively. These ambiguous cases arise as a result of inconsistencies between the classification implied by different line ratios and measurement uncertainties. About 13% of the LINERs and TOs in the HFS97 sample are in these ambiguous categories (and many more have uncertain classifications), which shows that the frontier between LINERs and TOs is a rather fuzzy one.

2.1. *LINERs, TOs, Weak– and Strong–[O I] Nuclei: Classification Issues*

In this paper we adopt a slightly different classification criterion for LLAGNs. While HFS97 divide LINERs from TOs at $[O\ I]/H\alpha = 0.17$, we prefer to place this dividing line at 0.25. To avoid confusion, we refer to sources with $[O\ I]/H\alpha \leq 0.25$ as "weak–[O I] nuclei" and sources with $[O\ I]/H\alpha > 0.25$ as "strong–[O I] nuclei." Our motivation to introduce these definitions is entirely empirical. We shall see that the $[O\ I]/H\alpha = 0.25$ limit represents much better the combined distributions of $[O\ I]/H\alpha$ and stellar population properties in LLAGNs. Clearly, this choice is largely irrelevant insofar as emission lines are concerned, since weak–[O I] nuclei still have $[O\ I]/H\alpha$ values intermediate between strong–[O I] and H II nuclei. In other words, weak–[O I] nuclei are essentially TOs and strong–[O I] nuclei are all LINERs.

Of the 162 LLAGNs in the HFS97 sample, 56 (35%) have $[O\ I]/H\alpha > 0.25$ and 106 (65%) have $[O\ I]/H\alpha \leq 0.25$. The corresponding fractions for our sample are nearly identical: 17 and 34 of our 51 LLAGNs fit our definitions for strong– and weak–[O I] nuclei, respectively.

2.2. *Comparison with the HFS97 Sample*

Although we have drawn objects exclusively from the HFS97 sample, it is important to evaluate whether we have introduced any bias in our sample selection. In Figure 1 we compare the distributions of distances (d) and morphological types (T) in these two samples. Triangles and circles correspond to strong– and weak–[O I] LLAGNs, respectively, and filled symbols mark objects that we have observed. The visual impression from the bottom left plot is that our galaxies are well mixed within the HFS97 sample. This is confirmed by the histograms projected along both axes of Figure 1, where we see that our galaxies (*filled areas*) follow reasonably well the distributions of d and T in the full HFS97 sample (*solid lines*). In both samples the distribution of morphological types of weak–[O I] nuclei is skewed toward somewhat later type hosts than for strong–[O I] nuclei, but with a substantial overlap, as discussed by Ho et al. (2003).

In Figure 2 we compare the G-band equivalent width and the $[O\ I]/H\alpha$ ratio, both extracted from HFS97. Again, one sees that our galaxies are well mixed within the HFS97 galaxies. This is confirmed by a statistical analysis. The mean value and rms dispersion of W(G band) is 4.6 ± 1.2 for all LLAGNs in HFS97 and 4.1 ± 1.3 in our sample. No biases were detected in the $[O\ I]/H\alpha$ ratio either (0.27 ± 0.21 compared to 0.25 ± 0.19 for the HFS97 sample and ours, respectively), and similar results apply to other stellar indices and emission-line ratios tabulated by HFS97. We thus conclude that our sample is representative of the full HFS97 sample in terms of emission-line and stellar population properties.

We note in passing that Figure 2 already gives away an important result of this investigation. Most objects with a weak G band are also weak [O I] emitters. The "inverted L" shape traced by the galaxies in this plot is only spoiled by a streak of three or four LINERs with $[O\ I]/H\alpha \sim 0.6$ and W(G band) < 4 Å. Apart from these objects, the top left region of Figure 2 is remarkably empty. Of the two objects that intrude most in this "zone of avoidance," NGC 5195 and IC 239, the latter has only an upper limit on [O I] and both have uncertain classifications (HFS97). Similar uncertainties affect several other points in Figure 2, but these do not affect the global shape of the distribution. Other versions of this plot are presented and discussed in § 6.

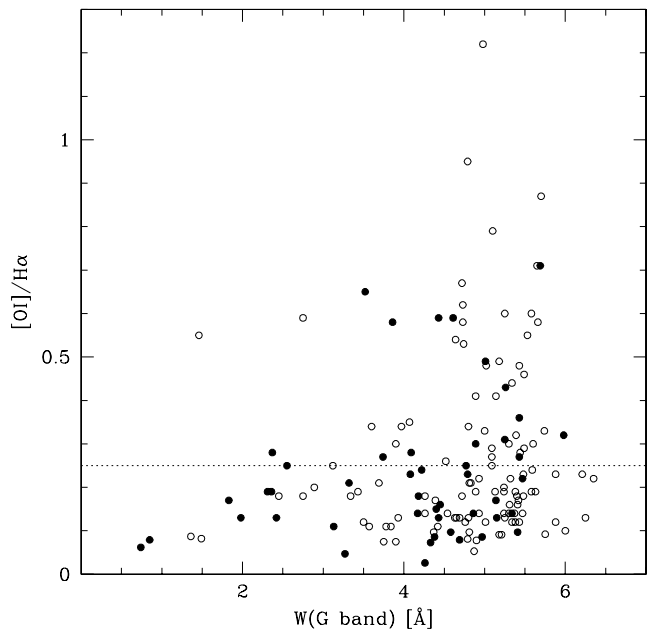

FIG. 2.—Equivalent width of the G band vs. $[O\ I]/H\alpha$ for LLAGNs in the HFS97 sample. Filled circles mark objects in our sample. The horizontal line at $[O\ I]/H\alpha = 0.25$ indicates our borderline between weak– and strong–[O I] nuclei. (All data are extracted from HFS97.)

TABLE 2

Log of Observations

Name	Telescope	Date	Exposure (s)	Air Mass	P.A.(field)
NGC 266.....	NOT	2001 Aug 21	3 × 1200	1.03	−79.6
NGC 315.....	NOT	2001 Aug 22	3 × 1200	1.11	−85.7
NGC 404.....	KPNO	2001 Jul 26	2 × 1200	1.29	0
NGC 410.....	NOT	2001 Aug 21	3 × 1200	1.13	−89.5
NGC 428.....	NOT	2001 Aug 23	4 × 1200	1.26	−42.2
NGC 521.....	NOT	2001 Aug 23	3 × 1200	1.69	−55.7
NGC 660.....	NOT	2001 Aug 21	4 × 1200	1.07	−49.5
NGC 718.....	NOT	2001 Aug 22	3 × 1200	1.20	−42.24
NGC 772.....	NOT	2001 Aug 23	3 × 1200	1.04	−52.9
NGC 841.....	NOT	2001 Aug 22	4 × 1200	1.02	−128.2
NGC 1052.....	NOT	2001 Aug 22	2 × 1200	1.26	−12.9
NGC 1161.....	NOT	2001 Aug 23	2 × 1200	1.06	−142.45
NGC 1169.....	NOT	2002 Nov 8	3 × 1200	1.05	−171.6
NGC 2681.....	NOT	2002 Nov 8	3 × 900	1.33	−98.5
NGC 2685.....	NOT	2002 Nov 8	3 × 1200	1.03	−12.7
NGC 2911.....	NOT	2003 May 3	3 × 1200	1.12	44.9
NGC 3166.....	NOT	2003 May 4	2 × 1200	1.11	8.4
NGC 3169.....	NOT	2003 May 3	3 × 1200	1.14	19
NGC 3226.....	NOT	2001 May 14	3 × 1200	1.05	−23.3
NGC 3245.....	NOT	2001 May 12	1800 + 1200 + 600	1.04	84.5
NGC 3627.....	NOT	2001 May 13	3 × 1200	1.09	42.6
NGC 3705.....	NOT	2001 May 14	3 × 1200	1.12	38.2
NGC 4150.....	NOT	2001 May 14	4 × 1200	1.28	87.6
NGC 4192.....	NOT	2001 May 12	4 × 900	1.04	25.8
NGC 4438.....	NOT	2001 May 15	4 × 1200	1.25	44.4
NGC 4736.....	NOT	2003 May 3	3 × 900	1.04	144.1
NGC 4569.....	NOT	2001 May 12	3 × 1200	1.11	48.7
NGC 4826.....	NOT	2001 May 14	3 × 1200	1.26	70.5
NGC 5005.....	NOT	2003 May 3	3 × 1200	1.09	106.6
NGC 5055.....	NOT	2001 May 15	4 × 1200	1.15	108.9
NGC 5377.....	NOT	2003 May 3	3 × 1200	1.24	108.6
NGC 5678.....	NOT	2001 May 13	4 × 1200	1.18	149.5
NGC 5879.....	NOT	2001 May 14	4 × 1200	1.21	133.3
NGC 5921.....	NOT	2001 May 12	3 × 1200	1.09	8.3
NGC 5970.....	NOT	2001 Aug 23	3 × 1200	1.19	54.1
NGC 5982.....	NOT	2003 May 4	3 × 1200	1.28	131.5
NGC 5985.....	NOT	2001 Aug 22	3 × 1200	1.29	128.8
NGC 6340.....	KPNO	2001 Jul 26	3 × 1200	1.34	0
NGC 6384.....	NOT	2001 May 13	3 × 1200	1.12	31.3
NGC 6482.....	NOT	2001 May 12	3 × 1200	1.03	−64.2
NGC 6500.....	NOT	2001 May 12	3 × 1200 + 900	1.02	17.2
NGC 6501.....	NOT	2001 Aug 22	3 × 1200	1.10	60.2
NGC 6503.....	NOT	2001 May 13	3 × 1200	1.33	−169.9
NGC 6702.....	NOT	2001 Aug 21	3 × 1200	1.06	155.5
NGC 6703.....	KPNO	2001 Jul 24	3 × 1200	1.03	0
NGC 6951.....	KPNO	2001 Jul 24	2 × 1200	1.21	0
NGC 7177.....	KPNO	2001 Jul 25	3 × 1200	1.20	0
NGC 7217.....	KPNO	2001 Jul 26	3 × 1200	1.01	0
NGC 7331.....	KPNO	2001 Jul 24	3 × 1200	1.03	0
NGC 7626.....	NOT	2001 Aug 23	3 × 1200	1.40	−57.4
NGC 7742.....	KPNO	2001 Jul 24	2 × 1200	1.10	0
NGC 3367.....	NOT	2001 May 13	3 × 1200	1.04	23.6
NGC 6217.....	NOT	2001 Aug 23	3 × 1200	1.62	140.8
NGC 205.....	NOT	2002 Nov 7	3 × 900	1.03	−152.8
NGC 221.....	NOT	2002 Nov 7	2 × 1200	1.22	−96.2
NGC 224.....	NOT	2002 Nov 7	2 × 900 + 600	1.08	−113.5
NGC 628.....	NOT	2002 Nov 7	3 × 1200	1.03	−12.7
NGC 1023.....	NOT	2002 Nov 7	3 × 900	1.10	113.7
NGC 2950.....	NOT	2002 Nov 7	3 × 900	1.21	−131.5
NGC 6654.....	NOT	2001 May 15	3 × 1200	1.41	−161.5

3. OBSERVATIONS

Observations were carried out in four runs at the 2.5 m Nordic Optical Telescope (NOT) and one run at the Kitt Peak National Observatory (KPNO) 2.1 m. The NOT observations used the ALFOSC detector with grism number 6 and a $1''$ wide slit, which gives a dispersion of 1.4 Å pixel^{-1} and covers the wavelength range 3500–5500 Å. The slit was oriented along the parallactic angle. Most observations were made under subarcsecond seeing and photometric conditions. The KPNO observations were carried out using the Gold Camera with grating 26 old and a slit $2''$ wide, which gives a dispersion of 1.24 Å pixel^{-1} and covers the 3400–5500 Å interval. The slit was oriented in the north-south direction, and the observations were done as close to the meridian passage as possible to avoid light losses by differential refraction. The weather during the observations was not photometric, and the seeing was typically $2''$–$3''$. A log of the observations is given in Table 2.

The data were reduced using standard IRAF procedures. The individual frames were overscanned, bias subtracted, and flat-field divided. The calibration also followed standard steps. The wavelength scale was calibrated using an HeNeAr lamp. The flux calibration was done with observations of spectrophotometric standard stars observed with a slit width of $10''$. The individual frames were combined using the *crreject* task in IRAF to remove cosmic rays. Sky was subtracted with the background task fitting a polynomial along the spatial light profile.

3.1. *Nuclear Extractions*

Most of the spectra have excellent signal out to several arcseconds from the nucleus. In Cid Fernandes et al. (2004, in preparation, hereafter Paper III) we explore this spatial information to map the stellar populations in the central regions of these objects, in analogy with previous work for type 2 Seyfert galaxies (Cid Fernandes, Storchi-Bergmann, & Schmitt 1998; Joguet et al. 2001; Raimann et al. 2003). In this paper we concentrate on the nuclear spectra. Off-nuclear extractions will only be used as templates for the nuclear spectra (§ 4).

Nuclear spectra were extracted from the central $1'' \times 1\farcs1$ (6 pixels) for the 52 galaxies observed at NOT and $2'' \times 2\farcs3$ (3 pixels) for the eight galaxies observed at KPNO. Using the distances in Table 1, the projected areas covered by these extractions correspond to radii of 11–204 pc, with a median value of 71 pc considering only the LLAGNs in the sample. The signal-to-noise ratio (S/N) was estimated from the rms fluctuation in the 4789–4839 Å interval, which is free of major absorption or emission features. We obtain S/N in the 23–88 range, with a median value of 50. In the 4010–4060 Å interval the median S/N is 22.

3.2. *HFS97 Extractions*

Most of the HFS97 spectra were collected through a $2'' \times 4''$ aperture, $\sim$7 times larger in area than our typical nuclear extractions. In order to allow a more meaningful comparison of our measurements with those in HFS97, we have also extracted spectra through a $2'' \times 4''$ aperture (hereafter the "HFS97 aperture"). This was straightforward for the KPNO observations, which have a slit width equal to that in HFS97. In order to construct an HFS97 aperture for the NOT data, which were collected through a $1''$ slit, we first extracted a $4''$ long spectrum and then multiplied it by 2 except in the nucleus (i.e., the inner $1\farcs1$), which was represented by an interpolation between off-nuclear extractions centered at $\pm 1\farcs1$ to avoid overweighting any nuclear point source. The flux in this approximate HFS97 aperture is typically 4 times larger than in our nuclear extractions.

All spectral properties discussed in § 5 were measured both through our nuclear extractions and through this HFS97 aperture, but only the nuclear values are published here, since except for galaxies with noticeable gradients (discussed in Paper III) the results are similar for both apertures. Tables for HFS97 aperture measurements are available upon request.

Besides spatial resolution, our observations differ from those of HFS97 in spectral coverage. The blue spectra in HFS97 cover the 4230–5110 Å interval, while our spectra go from 3500 up to 5500 Å. As well shall soon see, the region between 3500 and 4200 Å proved to be most revealing.

4. SPECTRA

In this section we present the spectra and two different methods to characterize the stellar populations in the central regions of LLAGNs. The first method consists of an empirical, qualitative classification based on the comparison with nonactive galaxies representative of simple stellar populations with different ages. The second method quantifies this classification by modeling the starlight using the nonactive galaxies as spectral templates. In § 5 we present measurements of several spectral indices (such as the 4000 Å break, Hδ, Ca II K, G band, and others), which provide yet another way to characterize stellar populations. A comparison of all these methods is important in view of the diversity of methods to analyze the stellar populations of AGNs found in the literature. This comparison allows us to do a relative calibration between them and can be used to convert the results obtained with one method to the others.

4.1. *Normal Galaxies and an Empirical Stellar Population Classification*

We start our presentation of the nuclear spectra by the nine nonactive galaxies in our sample, shown in Figure 3. The order of the spectra in this plot reflects approximately the age of the dominant stellar population, younger systems at the top. These normal galaxy spectra are used in this work as a reference basis for an empirical stellar population classification. Galaxies in Figure 3 can be separated into four classes:

1. Galaxies with evidently young ($<10^7$ yr) stellar populations (NGC 3367 and NGC 6217), characterized by a blue continuum and weak metal absorption lines.
2. Galaxies with a dominant intermediate-age, 10^8–10^9 yr population, characterized by pronounced HOBLs (NGC 205).
3. Galaxies with a mixture of intermediate-age and older stars (NGC 221 and NGC 628).
4. Galaxies dominated by an old stellar population (NGC 224, NGC 1023, NGC 2950, and NGC 6654), characterized by strong metal lines.

For short, these four stellar population classes are denominated *Y*, *I*, *I*/*O*, and *O*, respectively. We use the symbol η to denote these classes.

We have compared each of the LLAGNs in our sample to these normal galaxies and classified them in these same four stellar population categories according to a similarity criterion. This was first done by a simple visual inspection of the spectra and later confirmed by means of the starlight modeling scheme described in § 4.4. The results are listed in column (8)

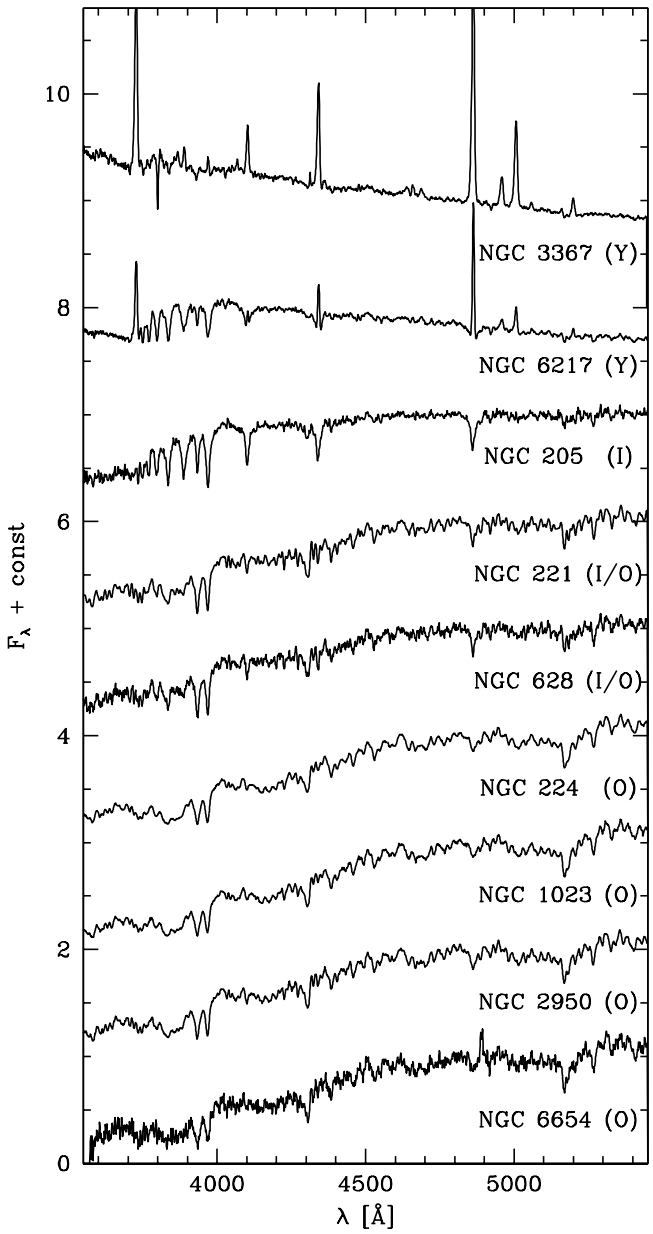

FIG. 3.—Spectra of the normal galaxies in the sample, including two starburst nuclei (*top*). Galaxies are sorted according to the age of the dominant stellar population, with younger systems at the top. *Y*, *I*, *I*/*O*, and *O* denote our empirical stellar population classes.

of Table 3. None of the objects resemble predominantly young systems like NGC 3367, so all our LLAGNs fall onto the $\eta = I$, I/O, and O categories.

This empirical classification provides a stellar population counterpart to the LINER/TO classification, which is based on emission-line properties. The η classes are used here just as a heuristic aid to sort the LLAGN spectra according to their main stellar populations. This is a useful strategy to investigate connections between emission-line and stellar population properties. However, classification criteria, while certainly helpful to identify general trends, have a certain degree of uncertainty and arbitrariness. When discussing our results we thus do not restrict ourselves to comparisons between discrete emission-line and stellar population classes. In § 6 we give more emphasis to comparisons between continuous stellar population and emission-line properties. We shall see that a clearer picture emerges if one avoids the rigidity of taxonomy.

4.2. *LINERs and Transition Objects*

The nuclear spectra for all LLAGNs in our sample are shown in Figures 3–7. Since our main aim in this paper is to investigate the relation between the stellar populations of these objects and their emission-line properties, we have split the spectra into six slots: strong–[O I] sources with either *O*, *I*/*O*, or *I* stellar population characteristics (Figs. 3 and 4) and weak–[O I] sources with either $\eta = O$, I/O, or I (Figs. 5, 6, and 7).

As is typical of LLAGNs, the spectra are completely dominated by starlight. With few exceptions (e.g., NGC 1052 and NGC 6501), emission lines are generally weak and sometimes altogether absent (e.g., NGC 410 and NGC 5055). Important diagnostic lines like Hβ and [O III] $\lambda\lambda$4959, 5007 are rarely seen, although [O II] λ3727 is detected in most spectra. As thoroughly discussed and illustrated by HFS97, starlight subtraction is an absolute necessity in order to measure emission lines in these objects, so we postpone the analysis of emission lines to a future communication. Except for [O II], line fluxes for galaxies in the present sample have already been measured by HFS97, including the important region around Hα, so we use their measurements when necessary. In the following we concentrate on the measurement and analysis of stellar population features.

As is evident from Figures 3–7, there is a clear connection between stellar population characteristics and the emission-line properties encoded in the weak/strong–[O I] classification. Old stellar populations are substantially more frequent in strong– than in weak–[O I] sources, whereas the opposite happens for stellar population class *I*. Numerically, we find that out of our 17 strong–[O I] nuclei, 10 (59%) are in the $\eta = O$ class, 5 (29%) have $\eta = I/O$, and only 2 (12%) belong to the $\eta = I$ class, while the corresponding numbers for the 34 weak–[O I] nuclei are 7 (21%), 11 (32%), and 16 (47%), respectively.

4.3. *High-Order Balmer Absorption Lines*

The most notable feature in this data set is the ubiquity of the H I high-order Balmer series in absorption (H8 and higher), particularly among weak–[O I] nuclei. By definition, objects where these features are clearly present are attributed to $\eta = I$ (i.e., they resemble NGC 205). Systems with HOBLs are also bluer and have shallower metal absorption lines than the rest. Overall, their spectra reveal clear signs of a 10^8–10^9 yr intermediate-age, "poststarburst" population. HOBLs may also be present in *I*/*O* nuclei, but blended with metal lines of old stars to such an extent that they do not stand out clearly in the total spectrum.

HOBLs have been seen before in a few LLAGNs, the most famous example being NGC 4569 (Keel 1996), which is also in our sample (Fig. 8*a*). However, an incidence rate as high as that suggested by our survey had not been suspected before. Ho et al. (2003) argue that objects like NGC 4569 are not representative of LLAGNs in their sample, most of which have a "demonstrably old" stellar population. While we agree that NGC 4569 is an extreme example and that old stars dominate the light in most LLAGNs, our spectra reveal the presence of intermediate-age stars in at least $\frac{1}{3}$ of the objects. The reason why we identify more of these populations than Ho et al. (2003) is that they had to base their judgment on the strength of

TABLE 3

STARLIGHT MODELING RESULTS

Galaxy (1)	x_Y (NGC 3367) (2)	x_I (NGC 205) (3)	$x_{I/O}$ (NGC 221) (4)	x_O (NGC 1023 + NGC 2950) (5)	A_V (mag) (6)	Δ (7)	η (8)
NGC 0266.....	0.1	5.2	17.8	77.0	0.18	2.8	*O*
NGC 0315.....	3.8	9.2	1.5	85.5	0.09	3.5	*O*
NGC 0404.....	0.0	78.5	0.0	21.5	0.90	6.6	*I*
NGC 0410.....	0.0	1.8	0.7	97.5	0.04	2.6	*O*
NGC 0428.....	0.0	49.8	0.0	50.2	0.31	8.7	*I*
NGC 0521.....	1.3	11.1	0.1	87.6	0.31	2.7	*O*
NGC 0660.....	0.0	59.4	0.0	40.6	2.38	11.7	*I*
NGC 0718.....	0.0	51.3	2.3	46.4	0.13	2.7	*I*
NGC 0772.....	32.1	10.9	24.4	32.5	0.38	1.8	*I*
NGC 0841.....	0.0	37.7	17.4	44.9	0.18	2.3	*I*
NGC 1052.....	16.5	0.0	0.5	83.0	0.57	3.0	*O*
NGC 1161.....	0.0	6.7	0.1	93.2	0.13	2.7	*O*
NGC 1169.....	0.0	0.0	48.2	51.8	0.26	5.7	*I/O*
NGC 2681.....	0.0	66.2	1.4	32.4	0.22	3.4	*I*
NGC 2685.....	0.3	0.9	50.5	48.4	0.21	4.9	*I/O*
NGC 2911.....	0.0	3.4	0.0	96.6	0.83	4.6	*O*
NGC 3166.....	0.0	28.8	9.4	61.8	0.19	2.3	*I/O*
NGC 3169.....	0.0	21.1	0.0	78.9	0.73	4.4	*I/O*
NGC 3226.....	0.0	2.7	0.0	97.3	1.08	4.2	*O*
NGC 3245.....	14.4	3.8	25.5	56.3	0.17	1.5	*I/O*
NGC 3627.....	0.0	66.6	1.4	32.0	0.47	3.0	*I*
NGC 3705.....	0.0	39.3	13.8	46.9	0.54	3.6	*I*
NGC 4150.....	0.0	66.8	32.0	1.2	0.00	6.5	*I*
NGC 4192.....	0.0	19.1	34.7	46.1	1.41	3.4	*I/O*
NGC 4438.....	0.0	2.6	50.9	46.5	1.48	2.9	*I/O*
NGC 4569.....	28.2	71.8	0.0	0.0	0.00	5.3	*I*
NGC 4736.....	0.0	48.8	0.0	51.2	0.07	2.3	*I*
NGC 4826.....	0.0	32.8	10.7	56.5	0.24	2.3	*I*
NGC 5005.....	0.0	45.1	0.4	54.5	0.77	3.7	*I*
NGC 5055.....	2.0	20.8	9.1	68.1	0.24	3.4	*I/O*
NGC 5377.....	0.0	76.8	0.1	23.1	0.02	2.5	*I*
NGC 5678.....	0.0	89.7	0.3	9.9	1.22	3.8	*I*
NGC 5879.....	0.0	52.0	0.9	47.1	0.46	7.3	*I/O*
NGC 5921.....	1.7	70.1	3.7	24.5	0.00	2.8	*I*
NGC 5970.....	0.0	5.7	56.4	37.9	0.13	4.6	*I/O*
NGC 5982.....	0.2	10.3	2.5	87.0	0.02	1.9	*O*
NGC 5985.....	0.0	6.8	34.4	58.8	0.19	4.9	*O*
NGC 6340.....	0.0	4.1	0.0	95.9	0.98	6.6	*O*
NGC 6384.....	1.2	2.2	61.3	35.3	0.02	4.4	*I/O*
NGC 6482.....	10.1	0.2	0.0	89.7	0.12	2.5	*O*
NGC 6500.....	24.7	0.1	4.0	71.3	0.08	2.3	*I/O*
NGC 6501.....	1.2	11.5	0.0	87.3	0.25	2.3	*O*
NGC 6503.....	22.5	55.8	16.3	5.4	0.32	3.0	*I*
NGC 6702.....	0.0	7.0	18.6	74.4	0.00	2.7	*O*
NGC 6703.....	0.0	3.4	0.0	96.6	0.22	3.5	*O*
NGC 6951.....	2.0	29.4	18.9	49.7	0.41	3.1	*I/O*
NGC 7177.....	2.4	13.7	43.1	40.8	0.39	2.8	*I/O*
NGC 7217.....	0.0	7.2	0.0	92.8	0.43	3.6	*O*
NGC 7331.....	0.0	5.3	15.0	79.8	0.37	2.8	*O*
NGC 7626.....	1.1	1.8	0.0	97.2	0.09	2.2	*O*
NGC 7742.....	0.0	14.3	0.0	85.7	0.16	4.1	*I/O*

NOTES.—Results of the starlight decomposition in terms of the normal galaxies NGC 3367, NGC 205, NGC 221, NGC 1023, and NGC 2950. Col. (1): Galaxy name. Cols. (2)–(5): x_Y, x_I, $x_{I/O}$, and x_O, given as percentage fractions of the flux at 4020 Å. Col. (6): *V*-band extinction of the best fit. Col. (7): Mean absolute percentage difference between the observed and model spectra: $\Delta = \left\langle \left| F_\lambda^{\rm obs} - F_\lambda^{\rm model} \right| / F_\lambda^{\rm obs} \right\rangle$. Col. (8): Stellar population class.

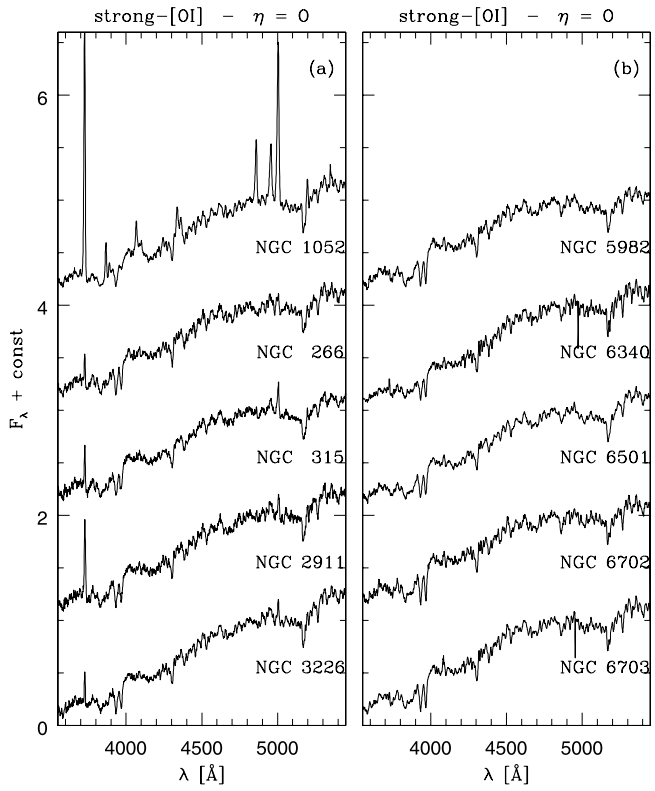

FIG. 4.—Nuclear spectra of strong–[O I] LLAGNs with predominantly old stellar populations ($\eta = O$).

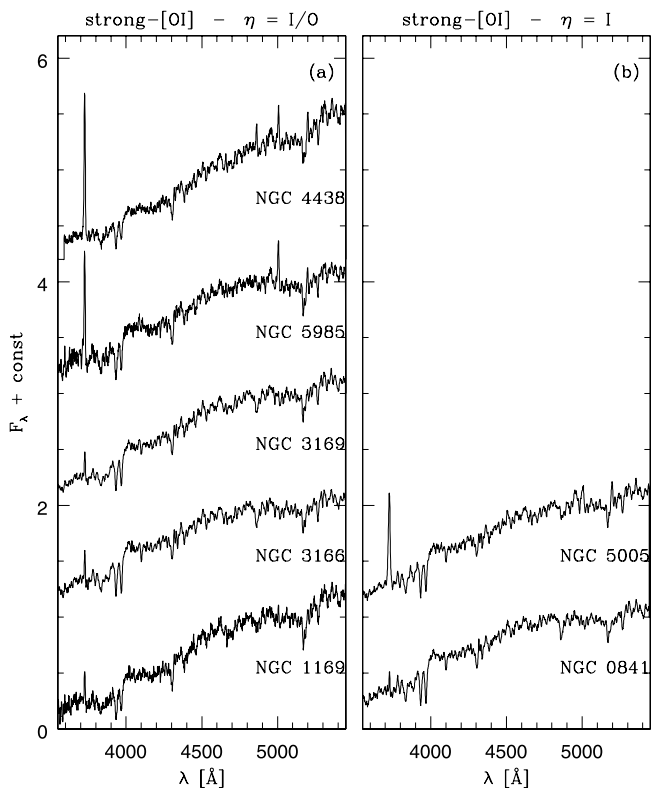

FIG. 5.—Nuclear spectra of strong–[O I] LLAGNs with stellar population classes (*a*) $\eta = I/O$ and (*b*) $\eta = I$.

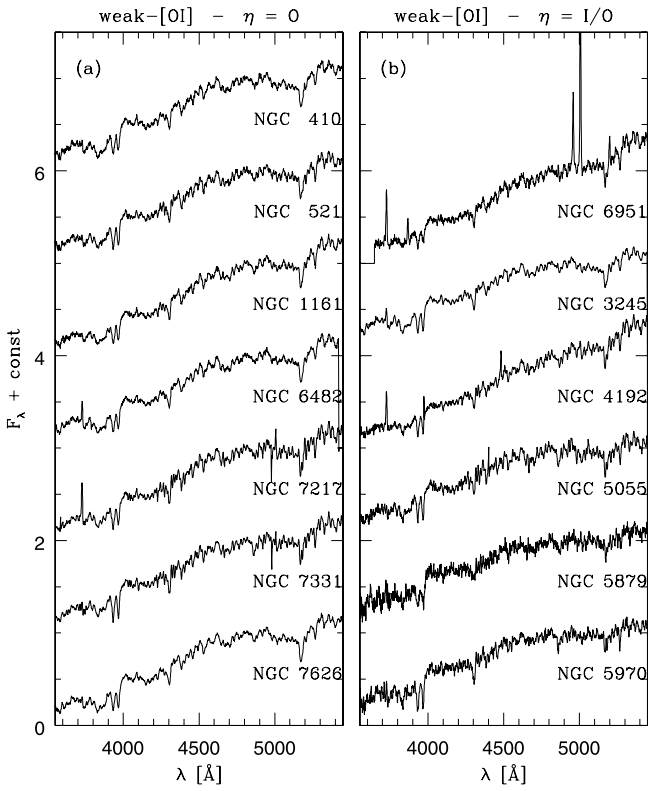

FIG. 6.—Nuclear spectra of weak–[O I] LLAGNs with stellar population classes (*a*) $\eta = O$ and (*b*) $\eta = I/O$.

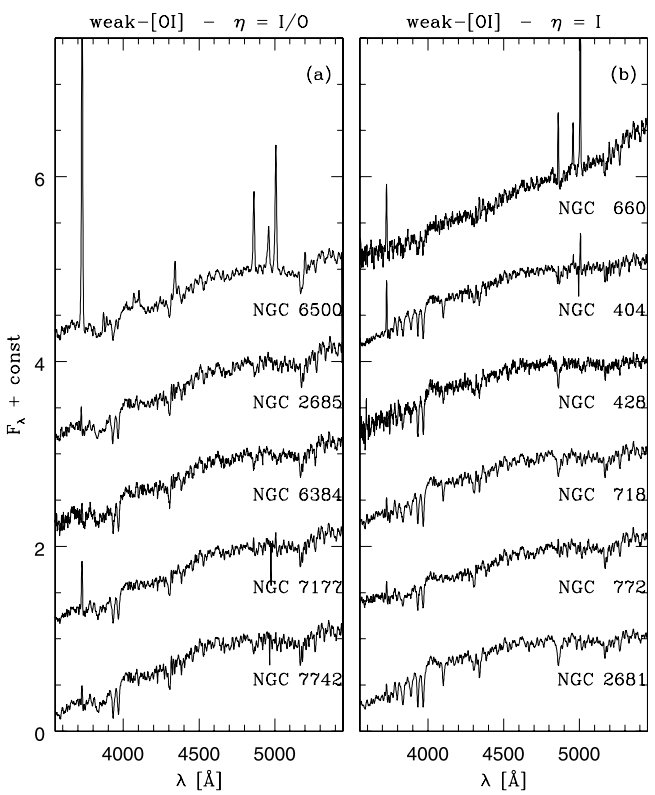

FIG. 7.—Nuclear spectra of weak–[O I] LLAGNs with stellar population classes (*a*) $\eta = I/O$ and (*b*) $\eta = I$.

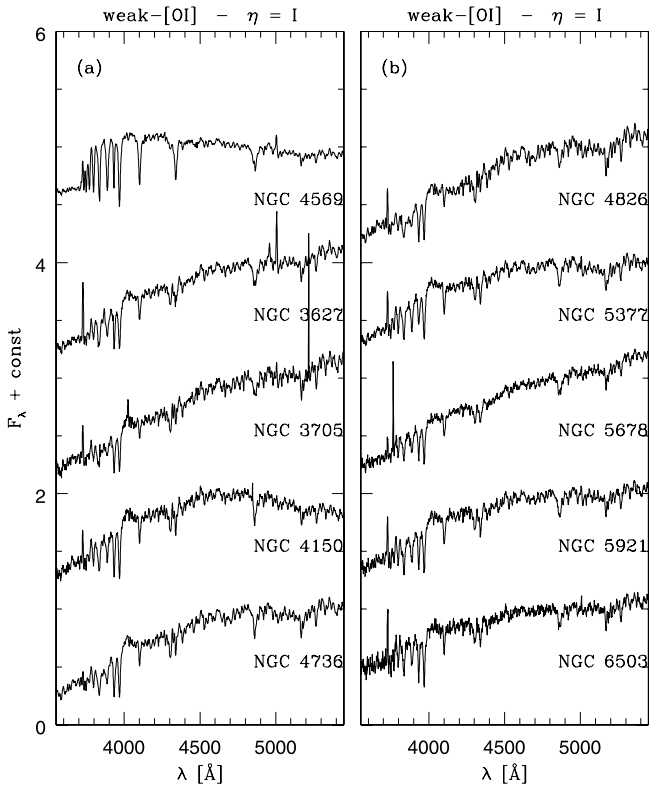

FIG. 8.—Nuclear spectra of weak–[O I] LLAGNs with a strong intermediate-age stellar population ($\eta = I$).

the Hγ, Hβ, and Hα absorptions, which are much more affected by emission and dilution by old stars than HOBLs.

As remarkable as the high frequency of HOBLs in weak–[O I] nuclei is their apparent dearth among strong–[O I] nuclei. HOBLs are $\sim$5 times more frequent in weak– than in strong–[O I] sources ($\eta = I$ fractions of $\sim$50% compared to $\sim$10%, respectively). These findings reveal a strong link between the central stellar populations and emission-line properties, particularly [O I]/Hα.

The statistics above obviously depend on our adopted borderline between weak– and strong–[O I] nuclei (at [O I]/Hα = 0.25), but the dichotomy persists (albeit somewhat diluted) even if one adopts the HFS97 [O I]/Hα = 0.17 classification criterion. A less classification-dependent assessment of the relation between stellar and emission-line properties is presented in § 6, where we replace the discrete stellar population and emission-line classes used above by a more continuous description.

4.4. *Empirical Starlight Modeling*

As noted in § 1, the location of TOs in between LINERs and H II nuclei in diagnostic diagrams suggests that their emission-line spectrum results from a mixture of AGN spectrum plus photoionization by young stars (HFS97). If this is the case, one would expect to find direct signatures of stellar populations of 10^7 yr or less in their spectra. Although the high incidence rate of HOBLs among weak–[O I] nuclei points to some sort of connection between stellar populations and emission-line properties, these features signal the presence of a $\sim 10^8$–10^9 yr poststarburst-like component, not a young starburst. The clearest single signature of young stars in the spectral range covered by our data is the W-R bump at 4680 Å. This feature is not evident in any of our LLAGN spectra. The W-R bump was only detected in the starburst galaxy NGC 3367 (Fig. 3), which is part of our comparison sample.

Given the dominance of old and intermediate-age stars in LLAGNs, a weak young starburst (with or without a correspondingly weak W-R bump) could well be lurking in some of our spectra. Detailed modeling of the stellar population mixture is required to evaluate this possibility. This modeling is performed in a separate communication (Paper II), in order not to mix data with models. In this paper we want to keep the analysis at a more empirical level. We have thus implemented an entirely self-contained starlight modeling technique that, instead of resorting to theoretical spectra, uses only our observed spectra.

Each spectrum was modeled as a combination of a base of template spectra. Two bases were considered: a "normal galaxy base," containing five spectra from our comparison sample (NGC 3367, NGC 205, NGC 221, NGC 1023, and NGC 2950), and an "off-nuclear base," containing two off-nuclear extractions centered at $\pm 2\farcs4$ from the nucleus. Except for the possibility of using off-nuclear templates, this procedure is very similar to the one employed by HFS97 in their starlight subtraction scheme.

All spectra were normalized to the flux at 4020 Å and corrected for Galactic extinction prior to the modeling. The A_B values of Schlegel, Finkbeiner, & Davis (1998), extracted from NED,[14] and the reddening law of Cardelli, Clayton, & Mathis (1989) were used for this purpose. Intrinsic extinction by a uniform screen of dust was allowed for. An algorithm was developed that searches for the combination of base spectra and extinction that best reproduces the nuclear spectrum of each LLAGN. The code was adapted from the empirical population synthesis (EPS) code of Cid Fernandes et al. (2001b) by simply replacing its spectral base by the full spectra in either one of these two bases. Regions around emission lines were masked out in the comparison between observed and model spectra. For the off-nuclear base, in most cases it was sufficient to mask out regions of 50 Å around [O II], Hβ, and [O III]. For the normal galaxy base we further masked regions around Hγ, Hδ, and [N I] λ5200 since these are rather strong in the spectrum of NGC 3367, included in this base to represent a young starburst.

The presence of an emission-line object in the normal galaxy base is another difference with respect to the starlight modeling scheme employed by HFS97. This difference is easily understood. HFS97 were interested in measuring emission lines from a starlight-free spectrum, so their starlight templates were constructed out of galaxies without emission lines. Our interest here is quite the opposite: we want to analyze the starlight itself, not the emission lines. NGC 3367 was introduced in the fitting to evaluate how strong a young starburst can be accommodated in our LLAGN spectra. A consequence of this choice is that our observed minus model residual spectra will have underestimated, emission-line fluxes when the NGC 3367 component is present in a significant proportion. There is no way of circumventing this without editing out the emission lines from NGC 3367 or resorting to theoretical stellar population spectra, since an emission-line–free starburst does not exist in nature. Nevertheless, in the majority of cases we find that the NGC 3367 component

[14] The NASA/IPAC Extragalactic Database (NED) is operated by the Jet Propulsion Laboratory, California Institute of Technology, under contract with the National Aeronautics and Space Administration.

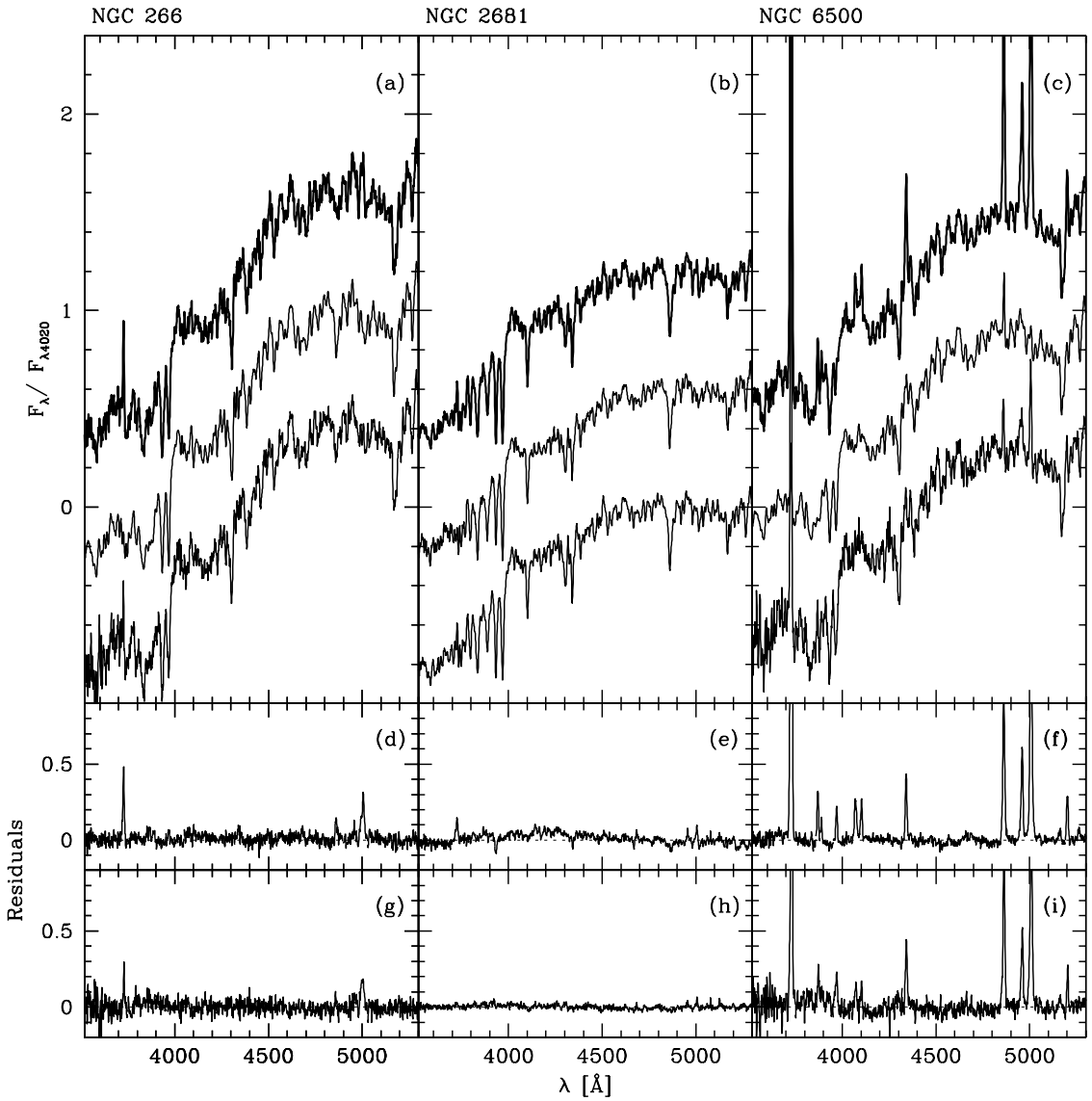

FIG. 9.—Results of the starlight modeling for NGC 266 ($\eta = O$, strong [O I]), NGC 2681 ($\eta = I$, weak [O I]), and NGC 6500 ($\eta = I/O$, weak [O I]). (*a–c*) Nuclear spectrum $F_\lambda^{\rm obs}$ (*top contour*) and two starlight models: $F_\lambda^{\rm temp}$ (*middle contour*), constructed out of linear combinations of the normal galaxies NGC 3367, NGC 205, NGC 221, NGC 2950, and NGC 1023; and $F_\lambda^{\rm off\text{-}nuc}$ (*bottom contour*), constructed combining two off-nuclear extractions. All spectra are normalized to the flux at 4020 Å, and the two models are shifted downward for clarity. (*d–f*) $F_\lambda^{\rm obs} - F_\lambda^{\rm temp}$ residual spectra. (*g–i*) $F_\lambda^{\rm obs} - F_\lambda^{\rm off\text{-}nuc}$. [*See the electronic edition of the Journal for a color version of this figure.*]

contributes very little ($\leq$2%) to the optical flux. In these cases, our residual spectra can be seen as pure emission spectra.

Examples of the results obtained with both spectral bases are shown in Figure 9. The top panels show the observed spectrum ($F_\lambda^{\rm obs}$; *thick line*) and the two models for the starlight spectrum. The middle spectrum shows $F_\lambda^{\rm temp}$, the template constructed out of linear combinations of the normal galaxy base, while the bottom spectrum ($F_\lambda^{\rm off\text{-}nuc}$) is the combination of two off-nuclear extractions that best matches the nuclear spectrum. Both models were shifted vertically for clarity. The residual spectra are shown in the bottom panels. Figures 9*d*–9*f* correspond to $F_\lambda^{\rm obs} - F_\lambda^{\rm temp}$, while Figures 9*g*–9*i* show $F_\lambda^{\rm obs} - F_\lambda^{\rm off\text{-}nuc}$. Except for regions containing emission lines, the typical difference between $F_\lambda^{\rm obs}$ and the $F_\lambda^{\rm temp}$ model is better than 3% for all cases shown. This is comparable to the noise level. Off-nuclear templates produce equally good results for the examples shown, with residuals of 4% for NGC 266 and NGC 6500 and 1% for NGC 2681. In some cases (e.g., NGC 772, NGC 4569, NGC 5921) the $F_\lambda^{\rm obs} - F_\lambda^{\rm off\text{-}nuc}$ residual reveals a nuclear blue component not present in the off-nuclear spectra. This happens especially in objects that have strong young and/or intermediate-age populations as revealed by the strength of the NGC 3367 and NGC 205 components in the normal galaxy decomposition. We also note in passing that Figure 9 shows that HOBLs are present not only in the nucleus of NGC 2681 but also in off-nuclear extractions. The region producing the HOBLs is therefore *spatially extended*, a result that is examined in more detail in Paper III.

One thus sees that, except for galaxies with noticeable gradients, both methods yield comparable accuracy. For our current purposes, the normal galaxy base is more relevant, since it provides a way of quantifying the stellar population mix in LLAGNs. In fact, this decomposition method provides

a quantitative basis for the comparative stellar population classification outlined in § 4.1. To illustrate how this works, one can write the relative contributions at $\lambda = 4020$ Å of NGC 3367 ($\eta = Y$), NGC 205 ($\eta = I$), NGC 221 ($\eta = I/O$), and NGC 2950 plus NGC 1023 ($\eta = O$) as a normalized four-component vector $\boldsymbol{x} = (x_Y, x_I, x_{I/O}, x_O)$. For the $\eta = O$ nuclei of NGC 266 and NGC 7626 we find $\boldsymbol{x} = (0\%, 5\%, 18\%, 77\%)$ and (1%, 2%, 0%, 97%), respectively, while for NGC 4438, which we classified as $\eta = I/O$, this vector is (0%, 3%, 51%, 46%), and for the $\eta = I$ nucleus of NGC 5921 we find (2%, 70%, 4%, 24%). In over 90% of the cases this scheme yields the same classification as that initially inferred by visual inspection of the spectra. In the few cases where a disagreement occurred, we adopted the visually estimated η class, although this has no consequence for the results of this paper.

The results of the starlight modeling in terms of the normal galaxy base are summarized in Table 3. A first important result of this analysis is that 23 of our 51 LLAGNs contain an NGC 205 component stronger than 20%. Except for NGC 5879, which has a noisy spectrum, all nuclei where $x_I > 30\%$ were classified as $\eta = I$ because of their conspicuous HOBLs. Between $x_I = 10\%$ and 30% some objects were classified as $\eta = I$ (NGC 772) and others as I/O (e.g., NGC 4192, NGC 5055). The starlight analysis therefore confirms the high incidence rate of HOBLs in LLAGNs, especially weak–[O I] sources, and helps to quantify the presence of these intermediate-age populations in cases where their contribution to the optical spectrum is not visually obvious.

4.5. *The Weakness of Young Stellar Populations in LLAGNs*

A second result of the starlight modeling is that few LLAGNs have an optically relevant young starburst. The contribution of the NGC 3367 component is larger than 20% in just four cases. In order of decreasing x_Y, these are NGC 772 (32%), NGC 4569 (29%), NGC 6500 (25%), and NGC 6503 (22%), which are all weak–[O I] sources.

Of all our LLAGNs, only NGC 6500 presents marginal evidence for the presence of the W-R bump. This can be seen by the coherent broad residual with amplitude of no more than a few percent in the $F_\lambda^{\rm obs} - F_\lambda^{\rm temp}$ residual spectrum in Figure 9*f*. Naturally, the amplitude of this residual increases a bit, removing the W-R bump from the NGC 3367 base component, but even then we cannot claim a conclusive detection of this feature. One way to double-check this possibility is to evaluate the residual spectrum obtained with the off-nuclear base. If W-R stars are concentrated in the nucleus, a W-R bump should appear in the $F_\lambda^{\rm obs} - F_\lambda^{\rm off\text{-}nuc}$ difference spectrum. In the case of NGC 6500, this residual reveals a weak narrow nebular He II λ4686 but no clear sign of a broad bump (Fig. 9*i*). A tentative detection of broad He II in this galaxy has been previously reported by Barth et al. (1997).

Detecting the W-R bump is already hard in bona fide starburst galaxies (e.g., Schaerer, Contini, & Kunth 1999), and the superposition of a dominant older stellar population only makes matters worse. In NGC 3367 this feature has an equivalent width of $\sim$5 Å, similar to the values in W-R galaxies (Schaerer, Contini, & Pindao 1999) and metal-rich giant H II regions (Pindao et al. 2002). Hence, an NGC 3367–like component diluted to less than 30% of the optical flux yields W-R bump equivalent widths of *at most* 1.5 Å, which is comparable to our spectral resolution, so weaker features are unlikely to be detected. The weakness of the young starburst component in LLAGNs may thus explain why we have not detected the W-R bump in our data.

It is therefore clear that young stellar populations contribute very little to the optical spectra of LLAGNs. It is important to point out that even when stars younger than 10^7 yr dominate the UV light, as in NGC 404, NGC 4569, NGC 5055, and NGC 6500 (Maoz et al. 1998), their contribution does not exceed 30% of the λ4020 flux. In fact, these young starbursts are not even detected in the optical for NGC 404 and NGC 5055 as a result of their *low contrast* with respect to older populations.

While current star formation seems to be proceeding at a residual level in LLAGNs, the ubiquity of intermediate-age populations indicates that it was much more prominent 10^8–10^9 yr ago, which points to a time-decaying star formation activity. This result contrasts with that obtained for studies of type 2 Seyfert galaxies, where young stellar populations are found in abundance (e.g., Cid Fernandes et al. 2001a; Joguet et al. 2001). The mean age of stars in the central regions of Seyfert 2 galaxies is thus smaller than that in LLAGNs. It is equally instructive to compare the stellar populations of weak– and strong–[O I] LLAGNs. The finding that intermediate-age populations are found almost exclusively among weak–[O I] nuclei implies that these sources are on average younger than those with strong [O I] emission. The implications of these results for evolutionary scenarios are considered in § 6 and Paper II.

5. SPECTRAL PROPERTIES

In this section we present measurements of a suite of stellar features in the nuclear spectra presented above. Measurements through the HFS97 aperture discussed in § 3.2 are only used here for comparison purposes. Tables with these and other measurements not published here are available upon request.

5.1. *Equivalent Widths and Colors in Bica's System*

In a series of papers starting in the mid-1980s, Bica and coworkers have explored a stellar population synthesis technique known as EPS, which decomposes a given galaxy spectrum in a combination of observed spectra of star clusters. In practice, instead of modeling the F_λ spectrum directly, this method synthesizes a number of absorption-line equivalent widths (W_λ) and continuum colors (C_λ), which are used as a compact representation of F_λ. EPS has proven a very useful tool in the analysis of galaxy spectra in a variety of contexts, from normal galaxies (Bica 1988) to starbursts (Raimann et al. 2000; Cid Fernandes, Leão, & Rodrigues-Lacerda 2003) and even AGNs (Schmitt, Storchi-Bergmann, & Cid Fernandes 1999; Raimann et al. 2003).

In this section we present measurements of W_λ and C_λ in Bica's system. These will be used here as raw measures of stellar population characteristics in our sample galaxies. These same data are used in Paper II as input for an EPS analysis. As a side step to this investigation, we have developed a fully automated scheme to measure W_λ and C_λ in this system. This is discussed next.

5.1.1. *Automated Measure of the Pseudocontinuum*

A drawback of Bica's system is its subjectivity. Both equivalent widths and colors are measured relative to a *pseudocontinuum* ($\rm PC_\lambda$), defined at preselected pivot wavelengths, which is traced interactively over the observed spectrum (see Cid Fernandes et al. 1998 for an illustrated discussion). Historically, this has limited the use of EPS to a

TABLE 4
WINDOW DEFINITIONS FOR THE PSEUDOCONTINUUM

Pivot λ (Å)	Interval (Å)	a_λ	b_λ
3660.....	3657–3667	0.0165	1.0069
3780.....	3775–3785	0.0130	1.0274
4020.....	4009–4020	0.0161	1.0019
4510.....	4501–4512	0.0820	0.9337
4630.....	4609–4627	0.1072	0.9037
5313.....	5307–5317	−0.0437	1.0507

NOTE.—The coefficient a_λ is in units of the median flux in the 4789–4839 Å interval used to normalize the spectra; b_λ is adimensional.

small number of researchers initiated in the "art" of drawing this continuum. Furthermore, the lack of an objective recipe to define PC_λ makes this whole system useless in the face of the huge spectral databases currently available, which must be processed in an entirely automated manner. The present data set is itself an example: counting all nuclear and off-nuclear extractions, there are over 700 spectra.

In order to remedy this situation, we have formulated an a posteriori definition of Bica's system. This was done by means of a straightforward computational procedure that mimics the placement of the pseudocontinuum, which until now has been carried out by hand.

We started by measuring by hand a representative subset of 42 spectra in the current data set, all normalized to the respective median flux in the 4789–4839 Å interval. For each pivot wavelength λ we have then computed *median* fluxes in windows of different sizes and locations. Windows were restricted to be at least 10 Å wide and centered within 100 Å of the corresponding pivot λ. The manually measured PC_λ fluxes were then compared to the automatically measured median fluxes (MF_λ) for all spectra, and a linear relation

$$PC_\lambda = a_\lambda + b_\lambda MF_\lambda \quad (1)$$

was fitted using an ordinary least-squares fit. The optimal window size and location were chosen to be those that produced the best linear correlation coefficient (i.e., smallest residuals). Window parameters and the corresponding MF_λ-to-PC_λ conversion coefficients a_λ and b_λ are listed in Table 4 for six pivot λ-values used in this work: 3660, 3780, 4020, 4510, 4630, and 5313 Å.

This recipe works extremely well, with linear correlation coefficients above $r = 0.97$ for all λ-values. Differences between manual and automated PC_λ measurements in our training set of 42 galaxies are of order 3%. This is well within the level of agreement between manual measurements of PC_λ carried out by different people (Cid Fernandes et al. 1998). We have further verified that the inclusion of other terms in equation (1) does not improve the fits significantly. Figure 10 illustrates the pseudocontinuum, as measured through our objective system. Equivalent widths are measured with respect to the continuum formed by linear interpolation between the PC_λ pivot points. The differences between W_λ measured with manual and automatic PC_λ are also of order 3%, being always smaller than 0.5 Å.

We thus conclude that we have succeeded in formulating a nonsubjective definition of the pseudocontinuum (and hence equivalent widths) in Bica's system, thus overcoming a long-held objection to this measurement system.

5.1.2. *Results*

We have measured seven equivalent widths in Bica's system: W_C, W_{wlb}, W_K, W_H, W_{CN}, W_G, and W_{Mg}. The window definitions for these absorption features are the same as defined in previous works (Bica & Alloin 1986; Bica, Alloin, & Schmitt 1994). Note that W_C is actually centered in a continuum region just to the blue of H9. In old populations, the spectrum in this region is well bellow the pseudocontinuum as a result of a multitude of weak metal lines, yielding $W_C \sim 4-5$ Å (e.g., NGC 266 and NGC 521 in Fig. 10). For populations of ∼1 Gyr or less, the continuum rises and W_C approaches 0, as seen in NGC 4150 and NGC 4569 (Fig. 10). For our sample, this index is a useful tracer of the presence of HOBLs. All cases where the HOBLs are visually obvious have $W_C < 3$ Å, while objects with $W_C > 4$ Å show no sign of these features. The W_{wlb} (where "wlb" stands for "weak-line blend") is centered on H9 but has a large value (similar to the Ca II K line, W_K) even in the absence of H9 because of the blend of many weak metal lines. Detailed discussions on the properties of these indices can be found in Bica et al. (1994) and Storchi-Bergmann et al. (2000).

In Table 5 we present the results for our nuclear spectra. The continuum colors PC_{3660}/PC_{4020} and PC_{4510}/PC_{4020}, corrected for Galactic extinction, are also listed. The uncertainties in all these spectral indices were estimated by means of Monte Carlo simulations. Each spectrum was perturbed 1000 times with Gaussian noise with amplitude equal to the rms fluctuation in the 4010–4060 Å interval. All indices were measured for each realization of the noise, and the 1 σ

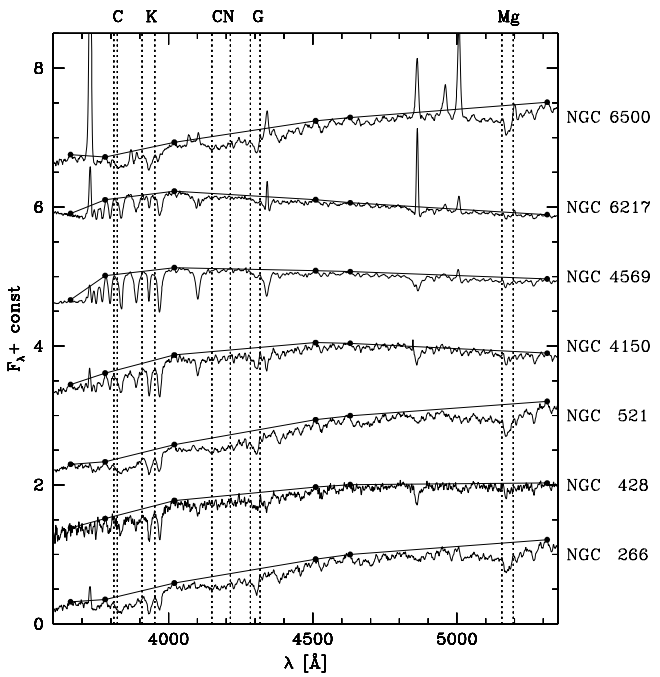

FIG. 10.—Examples of the pseudocontinuum in Bica's system, traced by the automatic method developed here (see text). Filled circles mark the pivot continuum points. Vertical dotted lines indicate windows of integration of some of the absorption features in this system. *Left to right*: W_C, W_K, W_{CN}, W_G, and W_{Mg}. [*See the electronic edition of the Journal for a color version of this figure.*]

TABLE 5

NUCLEAR SPECTRAL PROPERTIES

Galaxy (1)	W_C (2)	W_{wlb} (3)	W_K (4)	W_H (5)	W_{CN} (6)	W_G (7)	W_{Mg} (8)	F_{3660}/F_{4020} (9)	F_{4510}/F_{4020} (10)	$D_n(4000)$ (11)	$H\delta_A$ (12)	W(O II) (13)
NGC 0266.....	4.6	18.0	18.8	13.5	15.7	10.7	11.6	0.55	1.53	2.03	−2.1	5.4
NGC 0315.....	4.3	17.4	17.0	11.7	15.1	10.7	11.3	0.63	1.57	2.00	−2.8	8.1
NGC 0404.....	1.6	9.6	9.8	11.3	7.4	6.5	5.3	0.44	1.35	1.50	4.5	9.9
NGC 0410.....	4.9	19.4	17.6	12.9	17.6	10.6	12.9	0.60	1.55	2.13	−3.1	−1.0
NGC 0428.....	2.0	10.9	14.8	12.6	8.5	7.3	4.4	0.49	1.23	1.65	2.4	−1.7
NGC 0521.....	4.5	18.1	17.9	13.4	17.4	11.0	12.3	0.52	1.59	2.01	−2.7	−1.3
NGC 0660.....	1.3	10.8	14.5	11.5	7.3	7.5	7.1	0.47	1.71	1.72	−1.4	22.4
NGC 0718.....	2.6	13.1	13.1	12.9	9.5	8.3	7.7	0.52	1.30	1.65	3.1	1.0
NGC 0772.....	2.5	10.5	11.6	10.0	11.0	8.4	8.2	0.68	1.29	1.46	−0.3	0.8
NGC 0841.....	2.7	13.5	14.9	13.0	10.4	8.9	8.5	0.55	1.32	1.73	1.9	1.7
NGC 1052.....	4.5	15.8	17.3	8.2	18.1	9.9	11.1	0.63	1.61	1.88	−1.3	87.5
NGC 1161.....	5.0	19.4	19.0	13.8	18.5	11.6	12.2	0.56	1.63	2.16	−2.8	−1.7
NGC 1169.....	4.3	16.7	18.8	12.8	15.5	12.0	11.0	0.61	1.57	2.08	−2.4	7.3
NGC 2681.....	1.8	11.5	12.3	12.8	8.3	7.2	6.8	0.47	1.23	1.57	4.9	1.6
NGC 2685.....	5.4	17.6	18.7	13.6	15.0	11.6	10.1	0.55	1.53	2.01	−1.9	0.6
NGC 2911.....	4.2	18.4	17.7	13.5	17.7	10.9	11.2	0.51	1.68	2.05	−2.0	29.1
NGC 3166.....	3.2	15.2	15.9	13.0	12.1	9.4	8.5	0.53	1.39	1.80	0.8	4.7
NGC 3169.....	4.0	16.6	17.3	13.3	12.9	9.9	9.0	0.50	1.60	1.99	−0.4	6.2
NGC 3226.....	4.4	18.2	18.5	13.4	17.6	11.3	11.7	0.58	1.74	2.13	−2.4	7.7
NGC 3245.....	3.9	15.3	15.2	11.8	12.7	9.6	10.6	0.67	1.45	1.79	−1.5	1.7
NGC 3627.....	1.7	11.6	11.6	12.7	7.0	7.0	6.6	0.48	1.29	1.55	4.4	7.8
NGC 3705.....	3.0	12.9	14.8	13.1	10.1	8.7	7.6	0.49	1.40	1.73	2.2	4.0
NGC 4150.....	2.1	11.2	12.6	12.3	7.7	7.4	4.9	0.51	1.19	1.55	3.6	2.3
NGC 4192.....	3.0	15.3	16.0	10.9	11.8	9.0	9.5	0.53	1.76	1.93	0.1	13.4
NGC 4438.....	4.1	17.4	17.9	12.6	15.7	11.4	9.9	0.51	1.80	2.00	−1.9	57.8
NGC 4569.....	0.6	7.4	5.0	9.5	1.5	2.7	3.7	0.60	0.94	1.21	6.4	1.2
NGC 4736.....	2.6	13.6	12.9	12.3	9.9	8.4	7.6	0.53	1.29	1.67	2.8	−0.1
NGC 4826.....	2.7	15.2	14.4	12.7	13.2	9.6	9.1	0.52	1.41	1.76	1.0	4.6
NGC 5005.....	2.7	13.8	14.6	12.1	10.6	8.3	6.7	0.48	1.46	1.74	2.3	38.1
NGC 5055.....	3.8	15.1	14.1	11.9	15.1	8.7	10.5	0.54	1.47	1.75	−0.9	−1.3
NGC 5377.....	1.8	10.7	8.7	11.0	8.0	6.7	7.8	0.53	1.18	1.45	3.7	4.0
NGC 5678.....	1.1	7.8	8.7	10.3	3.8	6.0	5.6	0.49	1.40	1.48	3.6	−0.1
NGC 5879.....	3.2	11.7	16.3	12.7	8.8	8.7	7.5	0.48	1.33	1.72	0.8	3.2
NGC 5921.....	2.3	11.2	11.2	11.6	6.5	6.5	6.2	0.53	1.18	1.51	4.6	5.0
NGC 5970.....	4.1	14.5	18.4	13.3	10.1	10.2	8.0	0.61	1.40	1.86	−0.8	−2.5
NGC 5982.....	4.6	18.4	18.1	13.7	16.1	10.8	11.0	0.57	1.47	2.05	−1.9	−2.5
NGC 5985.....	4.0	15.5	18.9	12.1	13.2	10.6	9.6	0.59	1.51	1.97	−2.6	25.8
NGC 6340.....	4.9	18.1	20.0	14.3	17.1	12.1	11.2	0.49	1.92	2.26	−2.5	2.4
NGC 6384.....	4.9	15.2	18.6	12.9	10.3	10.7	9.9	0.66	1.45	1.92	−2.3	−2.7
NGC 6482.....	4.7	18.7	18.8	13.4	17.5	11.3	12.8	0.63	1.54	2.11	−2.7	4.4
NGC 6500.....	3.8	14.5	15.8	8.7	14.5	10.0	10.6	0.74	1.42	1.74	−4.3	98.2
NGC 6501.....	4.2	17.7	16.8	12.9	17.7	10.8	11.9	0.56	1.56	2.03	−2.2	−3.4
NGC 6503.....	1.3	7.9	9.5	10.4	4.3	5.8	6.2	0.67	1.15	1.36	2.9	4.5
NGC 6702.....	4.5	18.5	18.1	13.3	14.0	10.8	11.0	0.61	1.49	2.04	−1.7	−3.0
NGC 6703.....	4.8	18.7	18.5	13.8	16.3	11.5	11.5	0.56	1.60	2.11	−2.4	−1.9
NGC 6951.....	3.7	14.1	16.4	11.7	15.7	11.0	10.2	0.52	1.43	1.70	−0.2	21.3
NGC 7177.....	3.5	14.5	16.6	12.5	11.7	10.3	9.2	0.58	1.52	1.80	−1.3	11.2
NGC 7217.....	5.0	18.7	19.2	14.0	17.2	11.5	12.0	0.53	1.68	2.07	−2.6	12.2
NGC 7331.....	4.2	16.8	18.0	13.6	15.3	11.0	10.9	0.54	1.55	1.99	−1.0	−1.0
NGC 7626.....	4.9	19.2	18.1	13.9	17.9	11.0	12.6	0.58	1.58	2.12	−3.3	−1.2
NGC 7742.....	4.1	15.9	17.1	13.1	13.1	10.6	9.6	0.52	1.50	1.90	−0.9	2.2
NGC 3367.....	0.3	1.8	2.6	1.1	1.5	1.4	1.6	1.07	0.86	1.05	−3.0	13.3
NGC 6217.....	0.3	3.9	2.5	5.3	2.7	2.2	2.3	0.75	0.88	1.13	3.1	5.9
NGC 0205.....	1.2	8.4	7.1	11.5	4.3	5.2	3.3	0.51	1.07	1.37	6.3	−2.0
NGC 0221.....	4.0	15.5	17.9	13.9	11.9	10.6	8.1	0.60	1.41	1.86	−0.9	−3.4
NGC 0224.....	4.8	18.6	17.5	13.7	18.5	10.3	12.0	0.63	1.54	2.06	−2.9	−4.1
NGC 0628.....	2.9	13.1	16.1	12.7	8.5	8.5	6.8	0.64	1.35	1.74	0.5	−2.4
NGC 1023.....	5.4	20.8	19.4	14.5	19.1	11.9	12.3	0.57	1.63	2.26	−3.7	−4.6
NGC 2950.....	4.6	18.7	17.4	13.2	17.0	10.6	11.3	0.59	1.48	2.04	−2.0	−3.0
NGC 6654.....	4.7	16.4	18.5	13.4	16.6	12.5	12.1	0.61	1.58	2.09	−1.6	−5.4

NOTES.—Col. (1): Galaxy name. Cols. (2)–(10): Equivalent widths of seven absorption features and two colors, all in Bica's system. Col. (11): 4000 Å break index (Balogh et al. 1999). Col. (12): $H\delta_A$ equivalent width of Worthey & Ottaviani 1997. Col. (13): [O II] equivalent width of Balogh et al. 1999. All equivalent widths are given in Å.

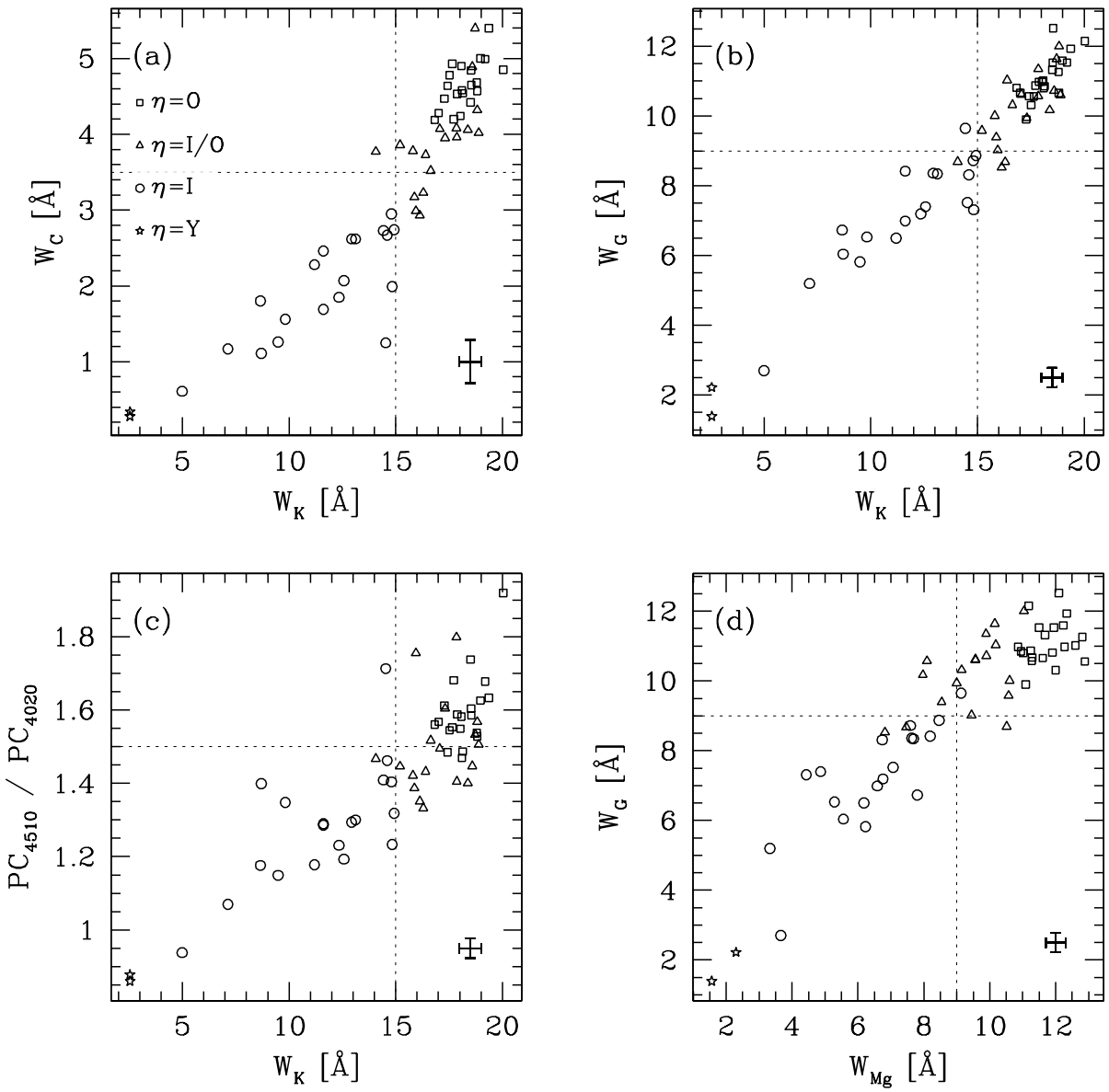

FIG. 11.—Relations between the equivalent widths of four absorption lines and one color in Bica's system. Empirical stellar population classes *Y*, *I*, *I*/*O*, and *O* are represented by different symbols. Squares, triangles, circles, and stars represent $\eta = O$, *I*/*O*, *I*, and *Y*, respectively. (The two stars correspond to NGC 3367 and NGC 6217, two starburst nuclei in our comparison sample.) Dotted lines approximately separate classes $\eta = Y$ and *I* from $\eta = I/O$ and *O*. Mean error bars are indicated in the bottom right corner of the figures. [*See the electronic edition of the Journal for a color version of this figure.*]

uncertainties were computed from the dispersion among the 1000 perturbed spectra. The median uncertainties are between 0.3 and 0.5 Å for all W_λ values and 0.03 for the PC_{3660}/PC_{4020} and PC_{4510}/PC_{4020} colors. The largest uncertainties are not more than twice these values.

In Figure 11 we illustrate the relation between the $\eta = Y$, *I*, *I*/*O*, and *O* empirical stellar population classes defined in § 4.1 and the equivalents widths W_C, W_K, W_G, and W_{Mg} and the PC_{4510}/PC_{4020} color. The correspondence is excellent, as can be appreciated by the locations of different symbols in all panels in this figure. Nuclei with young or intermediate-age populations are confined to the low-W_λ and blue color bottom left corners of Figures 11*a*–11*d*, while nuclei dominated by old stars populate the high-W_λ, red region, with $\eta = I/O$ objects in between. Approximate dividing lines can be placed at $W_C = 3.5$ Å, $W_K = 15$ Å, $W_G = 9$ Å, $W_{Mg} = 9$ Å, and $PC_{4510}/PC_{4020} = 1.55$.

Any of the W_λ values in Figure 11 can therefore be used as a continuous stellar population tracer that replaces our discrete *I*, *I*/*O*, *O* classification. In our previous study of the stellar populations in type 2 Seyfert galaxies (Cid Fernandes et al. 2001a) W_K was used in this way. Of all absorption features measured here, W_K is the strongest one, which makes it also the more precise in relative terms. Although the K line is actually produced by late-type stars, it indirectly traces younger populations by the dilution they cause on W_K. For this reason, in practice W_K is nearly as good a tracer of HOBLs as a more direct measure of these features, like W_C (Fig. 11*a*).

5.2. *Spectral Properties in HFS97's System*

HFS97 used a set of spectral indices (defined by Worthey 1992 and Held & Mould 1994) that also allow a characterization of stellar populations. Seven of the nine absorption equivalent widths and one of the two colors measured by HFS97 are

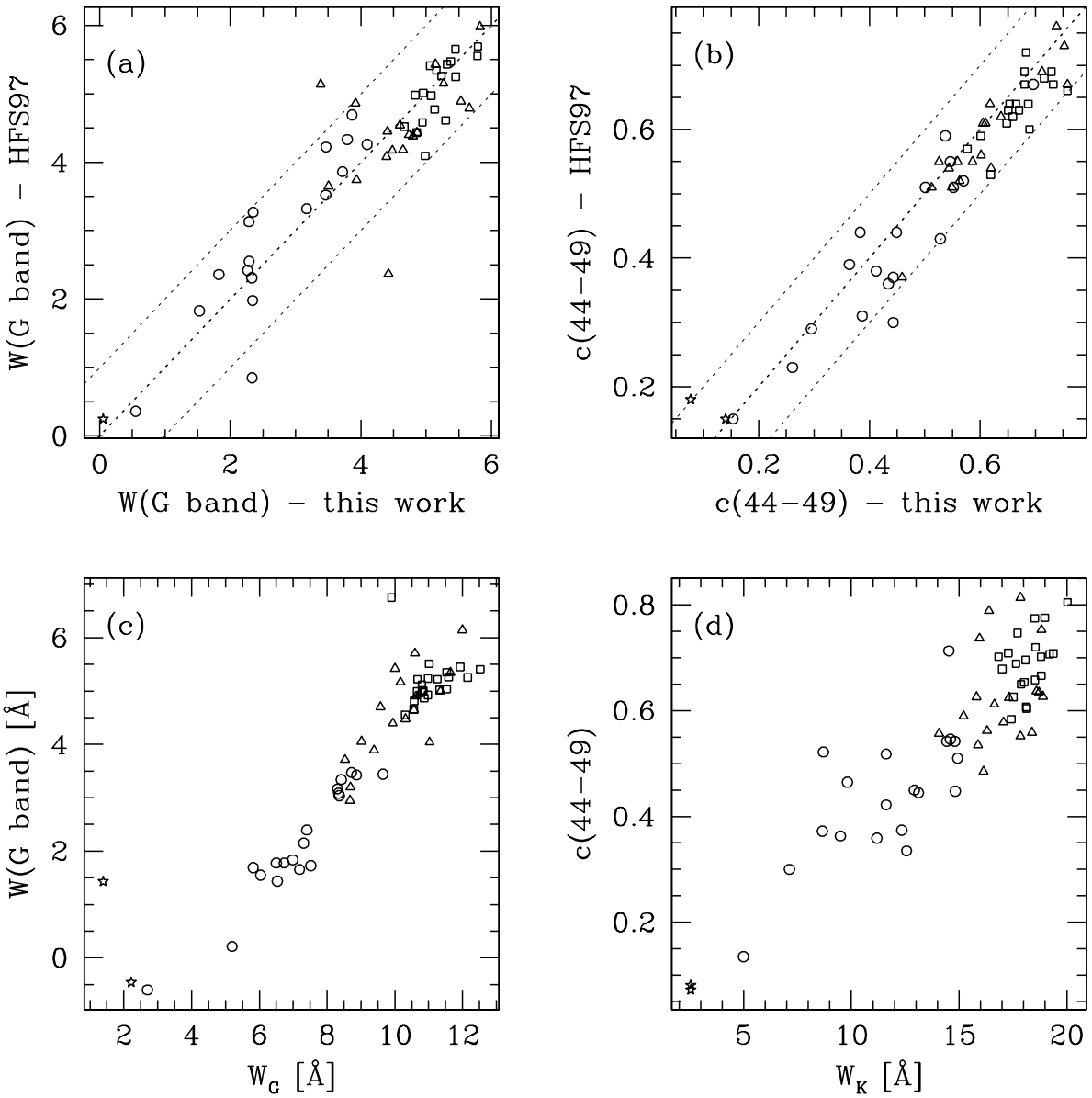

FIG. 12.—*Top*: Comparison of (*a*) the equivalent width of the G band and (*b*) the *c*(44–49) color for our HFS97 aperture spectra and the measurements of HFS97. Both indices were computed according to the definitions in HFS97. Diagonal lines indicate $y = x$ and the ± 2 σ range. *Bottom*: Relation between W_G and W_K, measured through Bica's system, and two HFS97 indices: (*c*) the G-band equivalent width and (*d*) *c*(44–49). Symbols as in Fig. 11. [*See the electronic edition of the Journal for a color version of this figure*.]

in the wavelength range covered by our data: the G band, Hγ, Fe λ4383, Ca λ4455, Fe λ4531, Fe λ4668, Hβ, and *c*(44–49). We have measured these indices in our spectra following the recipes in HFS97. This was done mainly for comparison purposes.

In Figure 12*a* we compare the equivalent width of the G band for our HFS97 aperture spectra with the measurements of HFS97. The mean difference is just 0.03 Å, and the rms is 0.6 Å, within the measurement errors of both studies. Similarly, Figure 12*b* compares the values of *c*(44–49) in these two studies. The difference in *c*(44–49) is just 0.03 ± 0.04, again within the errors.

In Figure 12*c* we compare the equivalent widths of the G band as measured in the HFS97 system and Bica's W_G, while in Figure 12*d* we plot the *c*(44–49) color against Bica's W_K. All quantities are measured from our nuclear spectra. The relatively tight relations between these independent measurements reinforce the impression from Figure 11 that different stellar indices in galaxy spectra are highly correlated. A corollary of these correlations is that a single index (say, W_K) is enough to provide a good first-order characterization of the stellar populations in our sample galaxies. This relatively high degree of redundancy in galaxy spectra is also detected by studies of principal component analysis (e.g., Schmidt et al. 1991; Sodré & Cuevas 1997), which show that a large fraction of the variance in galactic spectra is described by a single principal component. The physical property behind such an approximately monoparametric behavior is the *age* of the dominant stellar population (Schmidt et al. 1991; Ronen, Aragon-Salamanca, & Lahav 1999).

The strong interrelations between different stellar population indices can be used to extend results drawn from our sample to the full HFS97 sample. For instance, any correlation found between W_C or W_K and emission-line properties for our galaxies will also appear with the *W*(G band) HFS97

index, which has been measured by HFS97 for most of their 162 LLAGNs. Analogously, statistics related to our *Y*, *I*, *I*/*O*, and *O* stellar population classes can be readily extended to the full HFS97 sample exploring the relation between η and, say, W(G band).

5.3. *Other Spectral Indices: D_n(4000), Hδ_A and W(O II)*

Besides the Ca II K line and the HOBLs, the interval between 3500 and 4200 Å contains other features of interest. The 4000 Å break and Hδ, for instance, have been recently used as stellar population diagnostics for SDSS spectra of both normal and active galaxies (Kauffmann et al. 2003a, 2003b). We have measured these two indices for our spectra following the Balogh et al. (1999) definition of D_n(4000) and the Worthey & Ottaviani (1997) definition of Hδ_A. These are the same indices used in the SDSS work. We have not corrected Hδ_A for emission as this is insignificant for most of our LLAGNs. We further measured the [O II] equivalent width W(O II) according to the recipe of Balogh et al. (1999). All spectra were corrected for Galactic reddening prior to these measurements.

These indices are listed in columns (11)–(13) of Table 5. Note that H$\delta_A > 0$ corresponds to absorption while W(O II) > 0 corresponds to emission. Note also that negative W(O II) is obtained in many cases, but this does not necessarily mean a nondetection of [O II]. For instance, [O II] is clearly seen in the starlight-subtracted spectrum of NGC 7626, while the W(O II) index, which is measured over the total spectrum, yields -1.2 Å. As for other emission lines in LLAGNs, the accurate measurement of [O II] requires a careful starlight subtraction.

In Figure 13*a* we examine the relation between D_n(4000) and Hδ_A. The global distribution of LLAGNs in this diagram is similar to that obtained for SDSS galaxies (Kauffmann et al. 2003b). Interestingly, our $\eta = I$ LLAGNs, which are nearly all weak–[O I] sources, lie above the locus of steady star formation models of Kauffmann et al. (2003b), in a region occupied by galaxies that have experienced bursts of star formation in the past $\sim 10^9$ yr. This is consistent with the strong HOBLs found in these systems and the considerations of § 4.5. The location of $\eta = I$ weak–[O I] sources in Figure 13*a* is also similar to that of AGNs with $L_{[\mathrm{O\,III}]} < 10^7$ $L_\odot$ and TO-like emission-line ratios in Kauffmann et al. (2003a). Notwithstanding these similarities, it is important to observe that while the SDSS work pertains to scales of several kiloparsecs, our data trace stellar populations on scales of typically 70 pc.

Figure 13*b* illustrates the strong relation between Bica's W_{K} and D_n(4000), which is not surprising given that the W_{K} window is contained in the blue window of D_n(4000). The dashed line indicates the quadratic fit:

$$D_n(4000) = (1.013 \pm 0.006) + (0.031 \pm 0.001) W_{\mathrm{K}} + (0.00124 \pm 0.00007) W_{\mathrm{K}}^2. \quad (2)$$

6. THE LINK BETWEEN STELLAR POPULATION AND EMISSION-LINE PROPERTIES IN LLAGNs

Several times in § 4 we have noted an apparent connection between stellar population features revealed by our spectroscopy and the weak/strong–[O I] classification. In this section we use the spectral properties measured in § 5 in conjunction with the [O I]/Hα ratio from HFS97 to investigate this connection in a quantitative manner.

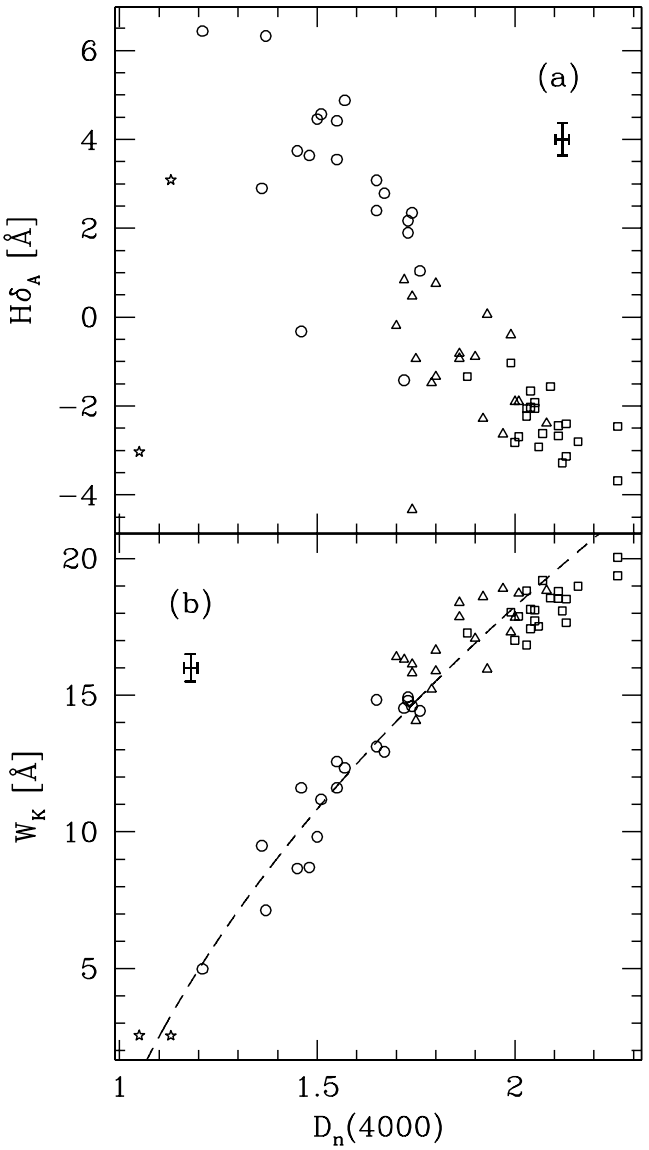

FIG. 13.—Relations between D_n(4000), Hδ_A, and W_{K}. Symbols as in Fig. 11. The dashed line in (*b*) shows a second-order polynomial fit. [*See the electronic edition of the Journal for a color version of this figure*.]

One way to investigate this relation more closely is to correlate [O I]/Hα with the W_{C} index, a useful tracer of the presence of HOBLs. The strong tendency of HOBLs to appear preferentially in weak–[O I] nuclei noted in § 4.3 should reveal itself as a correlation between [O I]/Hα and W_{C}. Similar correlations should exist between [O I]/Hα and the equivalent widths of metal absorption lines, since HOBLs come with an associated blue continuum that dilutes spectral features like the K line and the G band.

Figure 14 confirms these expectations. The figure plots [O I]/Hα against our nuclear measurements of W_{C}, W_{K}, W_{G}, and W_{Mg} (Table 5). What is seen in these plots is not so much a correlation in the sense of points scattered around a line, but a marked *dichotomy*: nearly all nuclei with weak absorption lines are weak–[O I] emitters, whereas nuclei with strong metal lines span the full range of [O I]/Hα. In graphical terms, the top left regions of all panels in Figure 14 are remarkably empty!

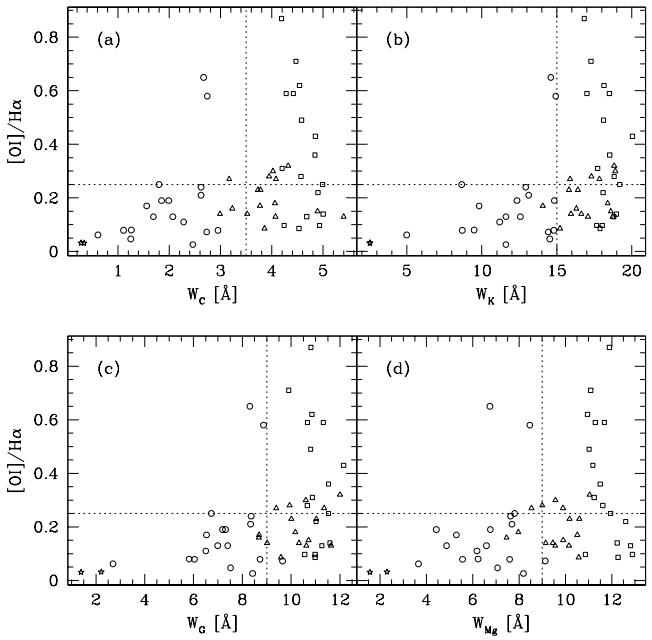

FIG. 14.—Comparison of absorption equivalent widths, which trace stellar populations, with the [O I]/Hα ratio, an AGN indicator. The [O I]/H$\alpha = 0.25$ borderline that separates weak– from strong–[O I] nuclei is indicated. The vertical dotted lines are the same as in Fig. 11; they separate objects with a strong intermediate-age population ($\eta = I$) from objects dominated by old stars ($\eta = O$). Symbols as in Fig. 11. [*See the electronic edition of the Journal for a color version of this figure.*]

This is not the first time in this paper that [O I]/Hα is plotted against a stellar population index. In Figure 2 we plotted [O I]/Hα versus W(G band) for the full HFS97 sample. There we see the same inverted L shape of any of the panels of Figure 14. Overall, these figures spell out a clear message: the narrow-line region of LLAGNs evidently knows what value of [O I]/Hα it can or cannot assume for a given stellar W_λ. This finding implies a strong connection between stellar populations and gas excitation processes in LLAGNs.

As suggested by the referee, an alternative reading of this result could be that galaxies with important circumnuclear star formation have an excess of Hα emission in the central few arcseconds (note that the [O I]/Hα values are from the $2'' \times 4''$ measurements by HFS97), resulting in a lower [O I]/Hα ratio. We have studied the aperture dependence of the Hα flux in order to check whether the link between [O I]/Hα and the stellar population is not a consequence of an excess of Hα flux in the larger HFS97 apertures, compared to the smaller apertures ($1'' \times 1\farcs1$) used in this work to derive the stellar population properties. We have retrieved from the *HST* archive STIS (G750M or G750L) spectra of 27 out of the 28 LLAGNs analyzed in Paper II. We find that Hα is very compact in all strong–[O I] LLAGNs. In weak–[O I] LLAGNs, the geometry of Hα is more diverse: in 7/22 Hα is compact, and in 14/22 more than 50% of the flux (measured through a $0\farcs2 \times 4''$ extraction) is inside the central $0\farcs2 \times 1''$. On the other hand, we find that the extension of the Hα emission does not correlate with the type of nuclear stellar population. In addition, we find that there is no correlation between the Hα luminosity and the [O I]/Hα ratio (both measured by HFS97). We thus conclude that the lower values of [O I]/Hα in weak–[O I] LLAGNs are not due to an excess of Hα emission provided by recent star formation in spatial scales of a few arcseconds.

A compelling visualization of the relation between [O I]/Hα and the stellar population properties is presented in Figure 15. In this figure we divide objects into bins in stellar W_λ, and within each bin we compute the fraction of objects with [O I]/H$\alpha < 0.17$ (*filled areas*), $0.17 \leq$ [O I]/H$\alpha \leq 0.25$ (*hatched areas*), and [O I]/H$\alpha > 0.25$ (*open areas*). The panels with W_K and W_C are for our sample, while the panel with W(G band) uses data tabulated in HFS97 for all their LLAGNs.

The predominance of weak–[O I] emitters among objects with low stellar absorption equivalent widths is obvious to the eye. Of the 19 LLAGNs with $W_K < 15$ Å, 17 have [O I]/H$\alpha \leq 0.25$. Similarly, 18 of the 21 nuclei with $W_C < 3.5$ Å have [O I]/H$\alpha \leq 0.25$. Hence, ~90% of objects with weak absorption lines are also weak–[O I] emitters. Note that the above limits in W_K and W_C correspond approximately to the borderline between our $\eta = I$ and $\eta = I/O$ or O stellar population classes (Fig. 11), so nearly identical statistics are obtained comparing η with [O I]/Hα. Likewise, since $\eta = I$ systems are also those with HOBLs, one can alternatively express the above statistics in terms of an [O I]/Hα–HOBL connection.

For the full HFS97 sample, ~80% of the W(G band) < 4.5 Å sources have [O I]/H$\alpha \leq 0.25$ (Fig. 15, *right panel*). This same fraction results if one uses the HFS97 measurements for the 51 LLAGNs in our sample, which reinforces our conclusion that there are no significant differential selection effects between the two samples.

It is important to draw attention to the fact that although most objects with HOBLs and diluted metal lines are weak in [O I], *the converse is not true*. There is a numerous population of weak–[O I] sources *without* conspicuous HOBLs and with stellar population indices typical of old, ~10 Gyr populations. Among objects with $W_K > 15$ Å, for instance, ~50% have [O I]/H$\alpha \leq 0.25$. These are the objects located at the bottom right corners of the inverted L distributions in Figures 2 and 14, also represented by the filled and hatched areas in the large-W_λ bins in Figure 15.

6.1. *Interpretation*

The shape of the distribution of points in Figure 14*b* lends itself to division into four regions, delimited by [O I]/Hα ~

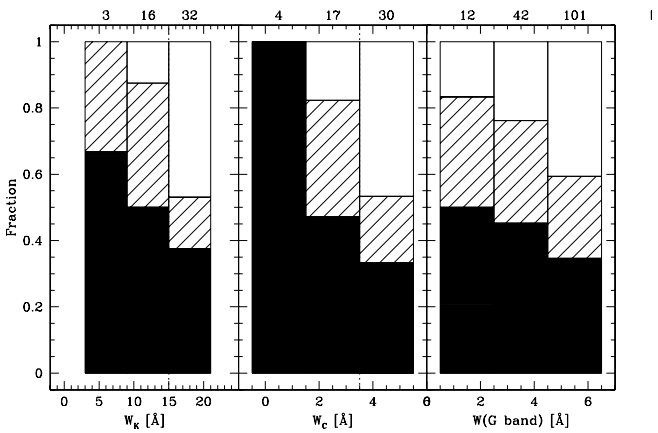

FIG. 15.—Fraction of objects in each of three ranges in [O I]/Hα as a function of different stellar absorption equivalent widths. Filled areas are used for [O I]/H$\alpha < 0.17$, hatched areas for $0.17 \leq$ [O I]/H$\alpha \leq 0.25$, and open areas for [O I]/H$\alpha > 0.25$. Numbers at the top indicate the number of objects in each W_λ bin. The left and middle panels are for the present sample of 51 LLAGNs, while the right panel is for the full HFS97 sample. [*See the electronic edition of the Journal for a color version of this figure.*]

0.25 in the vertical (emission line) axis and $W_K \sim 15$ Å in the horizontal (stellar population) axis. Similar divisions can be placed at $W_C \sim 3.5$ Å, $W_G \sim 9$ Å, and $W_{Mg} \sim 9$ Å in the other panels of Figure 14 and at W(G band) ~4.5 Å in Figure 2. The top left of these four quadrants is essentially empty. What kind of objects populate the remaining three quadrants?

Objects with clear signs of stellar populations of $\sim 10^9$ yr or less (i.e., those with HOBLs, diluted metal lines, and blue colors) all live in the bottom left quadrant. They are all weak–[O I] sources according to our definition. A plausible reading of this fact is that in these objects stars are directly linked to the gas excitation by some as yet undefined mechanism (see § 1 for a menu of possibilities), resulting in higher Hα per [O I] photon ratio than in strong–[O I] LINERs. These sources could be called "young TOs," where "young" actually refers to populations of 10^9 yr of less. Note that the stellar W_λ values in these sources are intermediate between those of starburst and early-type galaxies. In other words, they are transition objects also in terms of their stellar populations.

In the opposite end of the [O I]/Hα versus W_λ diagrams, stars cannot play an important role in the gas excitation, since photoionization by hot stars, be they young (i.e., a starburst) or old (post-AGB stars), produces smaller values of [O I]/Hα than observed in AGNs. The absence of optically significant $\lesssim 10^9$ yr populations corroborates this interpretation. Photoionization by an AGN is likely the dominant emission-line mechanism in these sources. Variations in nebular conditions or in the ionizing spectrum can be invoked to explain the range of [O I]/Hα values spanned by the data. A fitting denomination for nuclei in this top right quadrant is "old LINERs."

The bottom right quadrant of Figure 14 is populated by objects with TO-like emission-line spectra but no strong optical signs of young or intermediate-age stellar populations. These "old TOs" may well belong to the old LINER family, in which case their weak [O I]/Hα should perhaps be explained by an ionizing radiation field softer than for strong–[O I] LINERs. Alternatively, they may be simply weak young TOs whose $\lesssim 10^9$ yr stars are completely overwhelmed by the older population. This is likely the case of NGC 5055. The young starburst that clearly dominates the UV light of this galactic nucleus (Maoz et al. 1998) leaves no trace in the optical (Table 3), although our starlight decomposition indicates that 21% of the 4020 Å flux originates in an intermediate-age population. This nonnegligible contribution, however, causes little dilution of the metal lines. The bottom right quadrant of Figure 14 probably contains other such objects.

To summarize, our results suggest a scenario where stars younger than ~1 Gyr somehow participate in the gas ionization of young TOs, whereas in old LINERs an AGN is the dominant ionizing agent. The situation is less clear for old TOs, which may comprise a mixture of the above objects. Interestingly, "young LINERs" do not seem to exist. AGN taxonomy surely does not need more subclasses. Yet, LLAGNs have long been known to comprise a heterogeneous class, and, as discussed in § 1, models involving AGN- and stellar-driven ionization can both explain their emission-line properties. This empirically motivated scenario comes in the sense of trying to elucidate which of these two broad physical processes, AGNs or stars, best fits a given source. It is equally important to clarify that we do not claim young TOs to be AGN-less. After all, the current common wisdom is that all galaxies with bulges harbor an AGN, be it dead, alive, or somewhere in between. In young TOs the AGN contribution to the gas ionization would be small. Conversely, ionization by stellar processes in old LINERs would be overwhelmed by the AGN.

A potential caveat in identifying nuclei with weak metallic lines with stellar processes is that dilution by a quasar-like nonstellar continuum can also produce the same effect. Presumably, this should be more important for type 1 LLAGNs, i.e., L1.9 and T1.9 in the notation of HFS97. This effect indeed happens in *HST* spectra of some objects (Paper II). Interestingly, the two objects with W(G band) between 3.5 and 4 Å and [O I]/H$\alpha \sim 0.6$ in Figure 2 that intrude slightly into the zone of avoidance are NGC 841 and NGC 5005, both classified as L1.9. Although it is conceivable that this effect operates in a few cases, we find that type 1 and type 2 sources are well mixed in all our diagrams, so this cannot be a major effect in our ground-based observations. Furthermore, we point out that HOBLs were detected in both NGC 841 and NGC 5005, as well as in NGC 2681, another L1.9 with relatively weak metal absorption lines. It therefore seems more likely that the main diluting agent even in these type 1 LLAGNs is the continuum associated with stellar populations of $\lesssim 10^9$ yr rather than with a quasar-like continuum.

6.2. *Evolution and Contrast*

As time passes, HOBLs and the continuum of $\lesssim 10^9$ yr populations gradually disappear, and metal absorption features become progressively stronger. Passive evolution thus moves nuclei in left to right direction in Figures 2 and 14 on timescales of a few billion years. In the notation of the previous section, objects in the left half of Figures 2 and 14 are nearly all young TOs. If [O I]/Hα remains constant during this period, stellar evolution would gradually turn a young TO into an old TO. This would correspond to a horizontal evolutionary track onto any of our [O I]/Hα versus W_λ diagrams.

However, the hypothesis of constant [O I]/Hα does not seem warranted by the inverted L distribution of LLAGNs in Figures 2 and 14, which suggests that the presence of $\lesssim 10^9$ yr populations affects the [O I]/Hα ratio. For didactic purposes, let us consider a situation in which an AGN is entirely responsible for the production of [O I] photons, while Hα is produced both by the AGN and $\lesssim 10^9$ yr stars. In this case the stellar contribution to [O I]/Hα acts just in the denominator of this ratio. Evolution would thus move objects both to the right and upward along curved mixing lines in Figures 2 and 14 as the stellar-powered Hα emission fades. Considering that the AGN part of [O I]/Hα can assume a range of values (as a result of, e.g., different nebular conditions), one arrives at a scenario where stellar evolution takes points in the bottom left to any possible height in the right part of these figures. In other words, young TOs can end up as either old TOs or old LINERs.

It thus seems plausible that evolution plays a role in defining the looks of LLAGN spectra, in both their stellar and emission-line properties. Physical models for the evolution of [O I]/Hα must bear in mind that the intensity of [O I] is not only driven by the ionizing radiation field; it also depends strongly on the nebular geometry. Thus, variations of the ionization parameter and/or the density structure would also affect the [O I]/Hα ratio. Such variations may be tied to the evolution of stellar populations. In starbursts, for instance, [O I]/Hα is expected to increase with age as the bubble produced by the action of stellar winds and SNe expands (Stasinska, Schaerer, & Leitherer 2001; Stasinska & Izotov 2003).

Besides evolution, contrast effects must also be present, as can be illustrated by the case of NGC 6500. Judging by the relative contributions of the *Y*, *I*, and *I*/*O* components in our starlight decomposition (25%, 0%, and 4% of the 4020 Å flux, respectively), this is the youngest LLAGN in our sample. Yet, since 71% of the optical light comes from old stars, this galaxy does not quite make it into our observational definition of young TO, whereas from the above discussion of evolutionary effects one could naively expect it to be located at the bottom left of our [O I]/Hα versus W_λ diagrams. Further examples of contrast effects are NGC 5055 and NGC 404, whose optical spectra reveal no sign of the young massive stars unambiguously detected at UV wavelengths by Maoz et al. (1998). This starburst component is simply buried under the much stronger contribution of intermediate-age and older stars.

A quantitative assessment of these ideas is beyond the scope of this paper. Future communications will explore these issues by means of stellar population synthesis, spectral energy distribution modeling, and comparisons to Seyfert and starburst galaxies.

7. CONCLUSIONS

In this paper we presented the first results of a survey of the stellar populations of LLAGNs. Nuclear spectra covering the inner $\sim$70 pc in radius were presented for 51 LINERs and LINER/H II TOs plus a comparison sample of nine nonactive galaxies. The stellar population properties of LLAGNs were quantified by means of a comparison with nonactive galaxies, as well as by measurement of a suite of spectral indices over the 3500–5500 Å interval.

Our main results can be summarized as follows:

1. Young ($<10^7$ yr) starbursts contribute very little to the optical spectrum of LLAGNs. Even in the few nuclei known from UV observations to contain young massive stars, these populations participate with no more than 30% of the optical continuum light and sometimes are altogether undetected as a result of a much stronger contribution from other stellar populations.

2. Intermediate-age (10^8–10^9 yr) populations, on the other hand, are found in at least $\frac{1}{3}$ of all LLAGNs. These populations are easily characterized by pronounced H I Balmer lines in absorption, diluted metal lines, and relatively blue colors.

3. We found a very strong empirical connection between the stellar populations and emission-line properties of LLAGNs. Nearly all nuclei containing substantial populations of young and/or intermediate-age stars are weak–[O I] emitters, with [O I]/H$\alpha \leq 0.25$, whereas only $\sim$10% of the sources with stronger [O I] contain such populations. The mean stellar age of weak–[O I] LLAGNs is thus several billion years younger than that of strong–[O I] LLAGNs. Nuclei dominated by older stars, however, span the full range of [O I]/Hα values, from TOs to LINERs.

4. Given a few billion years, TOs with conspicuous intermediate-age populations will naturally evolve to either old TOs or old LINERs.

Perhaps the major lesson from this study is that the information contained in the stellar populations of active galaxies can provide valuable clues on the nature of these systems. Combining this information with emission-line data, we were able to establish an unequivocal connection between stellar populations and the gas excitation mechanism in LLAGNs. The physical origin of this connection, however, has not been unveiled in this work. By analogy with previous investigations (particularly of type 2 Seyfert galaxies), starburst activity is the prime contender to explain the relation between [O I]/Hα and stellar population properties reported in this work. Direct evidence for young stars in LLAGNs is nevertheless too scant to fully subscribe this interpretation at this stage, especially because other scenarios (such as SN shocks and photoionization by evolved poststarburst populations) may potentially explain our findings. Future papers in this series will address these and other related issues exploring complementary spectroscopic and imaging data, as well as detailed modeling of the stellar populations in these sources.

It is a pleasure to thank Grazyna Stasinska, Luis Colina, and Áurea Garcia Riessmann for their enlightening comments and suggestions and the referee for her/his suggestions that helped to improve the paper. R. C. F. and T. S.-B. acknowledge support from CNPq and CAPES. R. G. D. and E. P. acknowledge support by the Spanish Ministry of Science and Technology (MCYT) through grant AYA-2001-3939-C03-01. The data presented here have been taken using ALFOSC, which is owned by the Instituto de Astrofísica de Andalucía (IAA) and operated at the Nordic Optical Telescope under agreement between IAA and the NBIfAFG of the Astronomical Observatory of Copenhagen. We are very grateful to the IAA director for the allocation of 5.5 nights of the ALFOSC guaranteed time. The National Radio Astronomy Observatory is a facility of the National Science Foundation operated under cooperative agreement by Associated Universities, Inc.

REFERENCES

Alonso Herrero, A., Rieke, M. J., Rieke, G. H., & Shields, J. C. 2000, ApJ, 530, 688
Balogh, M. L., Morris, S. L., Yee, H. K. C., Carlberg, R. G., & Ellingson, E. 1999, ApJ, 527, 54
Barth, A. J. 2002, in ASP Conf. Ser. 258, Issues in Unification of Active Galactic Nuclei, ed. R. Maiolino, A. Marconi, & N. Nagar (San Francisco: ASP), 147
Barth, A. J., Reichert, G. A., Ho, L. C., Shields, J. C., Filippenko, A. V., & Puchnarewicz, E. M. 1997, AJ, 114, 2313
Barth, A. J., & Shields, J. C. 2000, PASP, 112, 753
Bica, E. 1988, A&A, 195, 76
Bica, E., & Alloin, D. 1986, A&A, 166, 83
Bica, E., Alloin, D., & Schmitt, H. R. 1994, A&A, 283, 805
Binette, L., Magris, C. G., Stasinska, G., & Bruzual, A. G. 1994, A&A, 292, 13
Bower, G. A., Wilson, A. S., Heckman, T. M., & Richstone, D. O. 1996, AJ, 111, 1901
Cardelli, J. A., Clayton, G. C., & Mathis, J. S. 1989, ApJ, 345, 245
Cid Fernandes, R., Heckman, T., Schmitt, H., González Delgado, R. M., & Storchi-Bergmann, T. 2001a, ApJ, 558, 81
Cid Fernandes, R., Leão, J. R. S., & Rodrigues-Lacerda, R. 2003, MNRAS, 340, 29
Cid Fernandes, R., Sodré, L., Schmitt, H., & Leão, J. R. S. 2001b, MNRAS, 325, 60
Cid Fernandes, R., Storchi-Bergmann, T., & Schmitt, H. R. 1998, MNRAS, 297, 579
Colina, L., González Delgado, R., Mas-Hesse, J. M., & Leitherer, C. 2002, ApJ, 579, 545
Donahue, M., & Voit, G. M. 1991, ApJ, 381, 361
Dopita, M. A., & Sutherland, R. S. 1995, ApJ, 455, 468
Engelbracht, C. W., Rieke, M. J., Rieke, G. H., Kelly, D. M., & Achtermann, J. M. 1998, ApJ, 505, 639
Falcke, H., Nagar, N. M., Wilson, A. S., & Ulvestad, J. S. 2000, ApJ, 542, 197
Ferland, G. J., & Netzer, H. 1983, ApJ, 264, 105

Filippenko, A. V. 1996, in ASP Conf. Ser. 103, The Physics of LINERs in View of Recent Observations, ed. M. Eracleous, A. Koratkar, C. Leitherer, & L. Ho (San Francisco: ASP), 17
Filippenko, A. V., & Terlevich, R. 1992, ApJ, 397, L79
Gonçalves, A. C., Véron, P., & Véron-Cetty, M.-P. 1999, A&A, 341, 662
González Delgado, R. M., Cid Fernandes, R., Pérez, E., Martins, L. P., Storchi-Bergmann, T., Schmitt, H., Heckman, T., & Leitherer, C. 2004, ApJ, 605, 127 (Paper II)
González Delgado, R. M., Heckman, T., & Leitherer, C. 2001, ApJ, 546, 845
González Delgado, R. M., Heckman, T., Leitherer, C., Meurer, G., Krolik, J., Wilson, A. S., Kinney, S., & Koratkar, A. 1998, ApJ, 505, 174
Halpern, J. P., & Steiner, J. E. 1983, ApJ, 269, L37
Heckman, T. M. 1980, A&A, 87, 152
———. 1996, in The Interplay between Massive Star Formation, the ISM, and Galaxy Evolution, ed. D. Kunth et al. (Gif-sur-Yvette: Editions Frontières), 159
Heckman, T. M., Armus, L., & Miley, G. K. 1990, ApJS, 74, 833
Heckman, T. M., Baum, S. A., van Breugel, W. J. M., & McCarthy, P. 1989, ApJ, 338, 48
Heckman, T. M., González Delgado, R., Leitherer, C., Meurer, G. R., Krolik, J., Wilson, A. S., Koratkar, A., & Kinney, A. 1997, ApJ, 482, 114
Held, E. V., & Mould, J. R. 1994, AJ, 107, 1307
Ho, L. C., Filippenko, A. V., & Sargent, W. L. W. 1993, ApJ, 417, 63
———. 1995, ApJS, 98, 477
———. 1997, ApJS, 112, 315
———. 2003, ApJ, 583, 159
Ho, L. C., et al. 2001, ApJ, 549, L51
Jiménez-Bailón, E., Santos-Lleó, M., Mas-Hesse, J. M., Guainazzi, M., Colina, L., Cerviño, M., & González Delgado, R. M. 2003, ApJ, 593, 127
Joguet, B., Kunth, D., Melnick, J., Terlevich, R., & Terlevich, E. 2001, A&A, 380, 19
Kauffmann, G., et al. 2003a, MNRAS, 341, 33
———. 2003b, MNRAS, 346, 1055
Keel, W. C. 1996, PASP, 108, 917
Maoz, D., Koratkar, A., Shields, J. C., Ho, L. C., Filippenko, A. V., & Sternberg, A. 1998, AJ, 116, 55
Nagar, N. M., Falcke, H., Wilson, A. S., & Ho, L. C. 2000, ApJ, 542, 186
Pérez, E., Márquez, I., Marrero, I., Durret, F., González Delgado, R. M., Masegosa, J., Maza, J., & Moles, M. 2000, A&A, 353, 893
Pindao, M., Schaerer, D., González Delgado, R. M., & Stasinska, G. 2002, A&A, 394, 443
Raimann, D., Storchi-Bergmann, T., Bica, E., Melnick, J., & Schmitt, H. 2000, MNRAS, 316, 559
Raimann, D., Storchi-Bergmann, T., González Delgado, R. M., Cid Fernandes, R., Heckman, T., Leitherer, C., & Schimitt, H. 2003, MNRAS, 339, 772
Ronen, S., Aragon-Salamanca, A., & Lahav, O. 1999, MNRAS, 303, 284
Schaerer, D., Contini, T., & Kunth, D. 1999, A&A, 341, 399
Schaerer, D., Contini, T., & Pindao, M. 1999, A&AS, 136, 35
Schlegel, D. J., Finkbeiner, D. P., & Davis, M. 1998, ApJ, 500, 525
Schmidt, A. A., Coppeti, M. V. F., Alloin, D., & Jablonka, P. 1991, MNRAS, 249, 766
Schmitt, H. R., Storchi-Bergmann, T., & Cid Fernandes, R. 1999, MNRAS, 303, 173
Shields, J. C. 1992, ApJ, 399, L27
Sodré, L., & Cuevas, H. 1997, MNRAS, 287, 137
Stasinska, G., & Izotov, Y. 2003, A&A, 397, 71
Stasinska, G., Schaerer, D., & Leitherer, C. 2001, A&A, 370, 1
Storchi-Bergmann, T., Cid Fernandes, R., & Schmitt, H. R. 1998, ApJ, 501, 94
Storchi-Bergmann, T., Eracleous, M., Livio, M., Wilson, A. S., Filippenko, A. V., & Halpern, J. P. 1995, ApJ, 443, 617
Storchi-Bergmann, T., Raimann, D., Bica, E. L. D., & Fraquelli, H. A. 2000, ApJ, 544, 747
Taniguchi, Y., Shioya, Y., & Murayama, T. 2000, AJ, 120, 1265
Terashima, Y., et al. 2000, ApJ, 533, 729
Worthey, G. 1992, Ph.D. thesis, Univ. California, Santa Cruz
Worthey, G., & Ottaviani, D. L. 1997, ApJS, 111, 377